FLOOD ROUTING THROUGH STORM DRAINS

Part III

EVALUATION OF GEOMETRIC AND HYDRAULIC PARAMETERS

by

V. YEVJEVICH and A. H. BARNES

November 1970

HYDROLOGY PAPERS
COLORADO STATE UNIVERSITY
Fort Collins, Colorado

45

FLOOD ROUTING THROUGH STORM DRAINS

Part III

EVALUATION OF GEOMETRIC AND HYDRAULIC PARAMETERS

by

V. Yevjevich and A. H. Barnes

HYDROLOGY PAPERS
COLORADO STATE UNIVERSITY
FORT COLLINS, COLORADO 80521

November 1970

No. 45

ACKNOWLEDGMENTS

The writers of this paper gratefully acknowledge the support and cooperation of the U. S. Bureau of Public Roads, Federal Highway Administration, in the research on flood movements through long storm drains conducted from 1960 to 1970. The writers also acknowledge the U. S. Public Health Service, National Institute of Health, for their additional support during 1962-64.

The initiative, cooperation and support given by Mr. Carl F. Izzard to this project on flood movement through storm drains is particularly acknowledged. Mr. Izzard, presently Director, Office of Development, Federal Highway Administration, U. S. Department of Transportation, was Chief, Hydraulic Research Division, U. S. Bureau of Public Roads at the start of the project. Further acknowledgment is extended to Mr. Charles F. Scheffey, Director, Office of Research, Federal Highway Administration, for his cooperation and encouragement. Dr. Dah-Cheng Woo, Senior Hydraulic Engineer, Federal Highway Administration, has cooperated extensively with this project. His reviews and suggestions pertaining to all reports, theses and other documents produced on the project have been particularly helpful.

Acknowledgment is given to Mr. William L. Lorah, Hydraulic Engineer, Wright Water Engineers, Denver, Colorado, for his contributions in the experimental study of the energy losses of junction boxes during his M.S. graduate work at Colorado State University in 1966. His advisor, Professor George L. Smith of the Civil Engineering Department, is also acknowledged. Several other graduate students, either through their thesis research or through direct work, contributed to the project. These theses and reports are listed in the bibliography of Hydrology Paper No. 44 under "Internal References." Dr. Shih-Tun Su, Post-Doctoral Fellow, Civil Engineering Department, Colorado State University, using existing data, assisted the writers in finishing this paper.

TABLE OF CONTENTS

LIST OF FIGURES AND TABLES

LIST OF FIGURES AND TABLES - Continued

ABSTRACT

The primary objective of this third part of a four-part series of hydrology papers on flood routing through storm drains is to present results on the investigation (experimental and analytical) of the geometric and hydraulic parameters of the experimental conduit; these parameters in turn define the coefficients in the two quasi-linear hyperbolic partial differential equations of gradually varied free-surface unsteady flow. As the accuracy of the evaluations of these parameters improves, the coefficients of the partial differential equations become more reliable. The final objective of this evaluation of parameters is to determine the extent to which the conduit geometry and hydraulic parameters influence the ability to predict the free-surface non-uniform steady or gradually varied unsteady flow, in a channel with a circular cross section.

The errors in cross section geometric parameters are analyzed in a conduit not ideally circular but approximated by an elliptical shape; errors are also analyzed when the undulations in the longitudinal slope of the conduit affect the predicted water surface profiles and thus the geometric parameters for a given water depth. The variation of hydraulic parameter of resistance, expressed by the Darcy-Weisbach friction factor, is experimentally determined and compared to the theoretical relation to Reynolds number. The friction factor may be satisfactorily expressed by the Prandtl-von Karman equation for turbulent smooth boundary. Energy losses in a 90 degree junction box are studied and relations are determined among the loss of power at the junction box, the ratio of the lateral inflow to the combined lateral and main inflow into the junction box, and the depth upstream from the junction box. The velocity distribution coefficients are shown to vary with the Darcy-Weisbach friction factor, and consequently, with the depth of flow. Boundary conditions for both controlled and free outfall are experimentally determined and approximated by power functions. Two types of steady non-uniform flow profiles, M1 and M2, are observed and analyzed as the initial conditions for the unsteady flow computations.

FLOOD ROUTING THROUGH STORM DRAINS

Part III

EVALUATION OF GEOMETRIC AND

HYDRAULIC PARAMETERS

by

V. Yevjevich* and A. H. Barnes**

Chapter 1

INTRODUCTION

1.1 Objective of Evaluation of Geometric and Hydraulic Parameters

The objective of evaluating various geometric and hydraulic parameters of an experimental conduit was to arrive at sufficiently accurate knowledge of the coefficients in the two partial differential equations of gradually varied free-surface unsteady flow in a storm drain. The conduit is described in detail in Part II of this series of four parts, (Hydrology Paper No. 44). The numerical integration of these two quasi-linear, partial differential equations can not produce accurate solutions if the coefficients of these equations are not sufficiently and reliably evaluated and expressed, with well estimated constants. These two partial differential equations in dimensionless form are (see Eqs. 3.23 and 3.19, Part I, Hydrology Paper No. 43):

$$\frac{A}{VB}\frac{\partial V}{\partial x} + \frac{\partial y}{\partial x} + \frac{1}{V}\frac{\partial y}{\partial t} = \frac{q}{VB} \qquad (1.1)$$

and

$$\frac{\alpha V}{g}\frac{\partial V}{\partial x} + \frac{\beta}{g}\frac{\partial V}{\partial t} + \frac{\partial y}{\partial x} = (S_o - S_f) - \beta\frac{Vq}{Ag}. \qquad (1.2)$$

The coefficients of these equations therefore, are A/VB, 1, $1/V$, and q/VB in Eq. 1.1., and $\alpha V/g$, β/g, 1, and $[(S_o - S_f) - \beta Vq/Ag]$ in Eq. 1.2. Using the Darcy-Weisbach equation for energy gradients, $S_f = fV^2/8gR$, and expressing the friction factor equation as a function of Reynolds number, $f = \psi(R_e) = \psi(VR/\nu)$, the parameters that appear in the coefficients of Eqs. 1.1 and 1.2 are: cross section area (A), water surface width (B), hydraulic radius (R), and the bottom slope (S_o), as geometric parameters, and the mean velocity ($V = Q/A$), lateral continuous inflow or outflow as discharge per unit length (q), friction factor (f), the velocity distribution coefficients (α and β), the kinematic water viscosity (ν) in the Reynolds number, and the gravitational acceleration (g), as hydraulic parameters. These parameters are constants or functions of either of the two or both of the dependent variables, the mean velocity V, and the depth y of the flow in the conduit. They may change also as the independent variables x and t change for given values of V and y. In general, the geometric parameters of cross sections and the longitudinal profiles of natural erodible channels change with the change of these two independent variables, the distance along the channel, and the time. The kinematic viscosity is a function of water temperature. Whatever the case may be, it is necessary to evaluate as accurately as feasible the geometric and hydraulic parameters that define the coefficients in the two partial differential equations as functions of any, several, or all of the four variables V, y, x and t, as functions of temperature, or as constant parameters.

One of the main objectives of the study of flood routing through storm drains is to compare analytical waves (numerically integrated) with physical waves (observed in the experimental facilities). The purpose of evaluating the parameters presented in this hydrology paper is to improve accuracy in computing the coefficients of the two partial differential equations, so that comparison of analytical and physical waves can be as accurate as practically feasible under the conditions of experimentation and research conducted in this study with well defined experimental facilities and conditions.

The comparison of computed depths of analytical waves and the observed depths of physical waves at any point in time and space depends, therefore, on the accuracy of the geometric and hydraulic parameters. The individual effects of errors in these parameters may tend to counter balance each other in the numerical solution of partial differential equations or they may tend to accumulate. For example, an estimated friction factor higher than the actual tends to increase the initial depths, and all depths in general, while an estimate of the cross sectional area greater than actual tends to produce computed depths of flow that are less than actual depths.

Justification and verification of a theoretical hypothesis depend on the agreement between the predicted and the observed results. Any disparity between the computed and measured values must be due to basically two influences. The first influence includes limitations of the theoretical analysis of waves and its computational methods of integration. The second influence includes limitations in physical measurements and the impossibility of total precision

* Professor-In-Charge of Hydrology and Water Resources Program, Dept. of Civil Engineering, Colorado State University.

**Associate Professor of Civil Engineering, Colorado State University.

in determining the parameters that define the coefffi-cients of partial differential equations.

The objective of the discussion in the following chapters is to provide an evaluation of the significant physical parameters (either as constants or as functions of velocity and/or depth), which enter into the coefficients of differential equations of gradually varied free-surface unsteady flow. These evaluations are based on the same experimental system in which the physical waves are observed. Thus, the discrepancy between computed and observed results could be caused by random errors rather than by systematic errors in parameter evaluations.

In any applied situation, the analyst and the designer must estimate values of the appropriate geometric parameters, friction factors, local energy losses, velocity distribution coefficients, and boundary and initial conditions. The differences between computed and observed results include both the systematic errors of estimation and the random errors of observation. The effect of systematically varying the hydraulic parameters with regard to the resulting analytical waves has been also studied and is both briefly mentioned in this paper, and discussed in detail in Part I, Hydrology Paper No. 43.

Another objective of this investigation of geometric and hydraulic parameters is to provide insight into the various sources of uncertainties in the numerical solutions of analytical waves, which result from the uncertainties in coefficients of partial differential equations. The potential experimental research that could improve knowledge about the coefficients in the two partial differential equations of unsteady flow may be also inferred from the results presented.

1.2 Evaluation of Parameters Under the Conditions of Gradually Varied Free-Surface Unsteady Flow

In general, parameters such as friction factors and velocity distribution coefficients as functions of Reynolds number for hydraulically smooth boundaries should be different in unsteady flow and steady flow, because of the differences in boundary layers of a steady and unsteady flow. These differences should be larger if a wave is less gradually varied. No attempt was made in this study to find whether there are significant differences in friction factors between gradually varied unsteady-flow conditions and corresponding steady-flow conditions. No significant difference could be detected, as discussed in Chapter 3. Because the experiments related to particular experimental facilities and instrumentation did not permit a detection of significant differences in the friction factor between the gradually varied waves and the steady flow, the influence of unsteadiness on velocity distribution coefficient was not studied either.

The results and discussions presented in the following chapters refer to steady flow conditions, under the general assumption that the relations obtained for parameters in steady flow are sufficiently accurate for gradually varied waves. Also, as it is shown in Part I, Hydrology Paper No. 43, the small relative errors in friction factor (f) and in the velocity distribution coefficients (α,β) result in still smaller relative errors in the water depths of numerically integrated partial differential equation of given waves.

1.3 Specifications about Geometric and Hydraulic Parameters that Define Coefficients of the Two Partial Differential Equations

The geometric parameters depend on the depth y (as one of the two dependent variables in partial differential equations) for a circular prismatic conduit and are constants along the conduit and in time for a given depth. The geometric parameters A, B, and R, or the area, surface width, and hydraulic radius, respectively, must be known as functions of depth for input into Eqs. 1.1 and 1.2. The bottom slope (S_o) as another geometric parameter is an arbitrary parameter. It is constant in this study for any given run, and is assumed independent of any other variable or parameter. The area (A) and the surface width (B) are functions of the depth (y) only. As the energy gradient (S_f) is a function of the hydraulic radius (R), and as $R = A/P$, with P the wetted perimeter, it is necessary to know $A(y)$ and $P(y)$ and through them $R(y)$. The errors in the measurement of depth (y), the non-circularity approximated by the ellipticity of the conduit in this study, the angle of the minor axis of the fitted ellipse with the vertical (tilting of the ellipse), the errors in the conduit diameter (D), and the undulations in the bottom slope (S_o), all affect the accuracy of the three parameter functions, $A(y)$, $P(y)$, and $R(y)$, which define the coefficients of the partial differential equations. The computation of these three functions and the errors involved are defined in this paper under evaluation of geometric parameters. Chapter 2 is concerned with the geometric parameters of the experimental conduit, particularly the discussion of effects of errors in depth, errors due to approximate ellipticity, inclination of the elliptic profiles to the vertical, errors in conduit diameter, and effects of the undulation of the invert of the straight aligned conduit.

It was necessary to obtain by experiments the relation between the friction factor and the Reynolds number, instead of using a constant friction factor of rough pipes, because the energy loss measurements in the experimental conduit have shown the conduit to be a smooth boundary pipe. The evaluation is given in Chapter 3 using the Darcy-Weisbach friction factor (f) as the measure of the smooth boundary roughness.

Apart from the resistance to flow of the smooth conduit boundary, resistances may occur in the form of additional energy losses at sudden changes in the geometry along the conduit. All losses at short structures along the conduit, which deviate from the circular prismatic conduit, may be encompassed as losses at geometric singularities. The only important singularity studied for energy losses was the junction box where the lateral inlets join the main conduit and produce additional energy losses, both because of the geometry of the junction box and because of the inflow from the lateral inlets into the main flow. These losses are studied both an a small model and in the experimental conduit and are described in Chapter 4. The experimental facilities used to determine the results are described in Part II, Hydrology Paper No. 44.

The two velocity distribution coefficients, α and β, enter into the coefficients of partial differential equations. Experimental study has been carried out in the main conduit of the experimental facility to determine both the variation of these coefficients with hydraulic parameters and their

approximate and constant representative values. The procedure and the results are described in Chapter 5.

It can be stated that no numerical solution of partial differential equations of gradually varied free-surface unsteady flow is reliable without accurate evaluation of the corresponding boundary and initial conditions. Chapter 6 and 7 describe the analysis and experimental results in establishing reliable boundary and initial conditions of the experimental conduit for the objectives of this study.

Because the temperature of water in the experimental conduit drawn from the bottom of the Horsetooth Reservoir near the CSU Engineering Research Center was constant (about $50^{o}F$) during experiments, the variations of kinematic viscosity (ν) with temperature, and through it the variation of R_e, f, α, and β with temperature were not studied.

1.4 Lateral Inflows

The lateral inflows into storm drains, or the outflows out of them, may be either concentrated at points or distributed along them. In most cases the inflows into storm drains are concentrated at junction boxes. Also, in a majority of cases the outflow is concentrated at some main points of a drain. However, cases can be conceived where some inflows into storm drains may be continuous along a conduit (longitudinal drainage of ground water), and the outflow may be continuous either as the longitudinal seepage out of the drain or as the spillover along the top of a drain. Equations 1.1 and 1.2 are designed to deal with these continuous inflows or outflows, with q measured in discharge per unit length of a drain. This case was not investigated in this study, however. In other words, the potential physical inflows or outflows as discharges per unit length of the storm drain have not been evaluated, and the influence of errors in these flows in the comparison between the analytical and physical waves has not been studied. Therefore, the coefficients q/VB in Eq. 1.1 and $\beta Vq/Ag$ in Eq. 1.2, with q the distributed lateral inflow, were not investigated.

The known concentrated lateral inflows are studied by considering their boundary conditions effects on Eqs. 1.1 and 1.2, without requiring the study of any new geometric or hydraulic parameter. Chapter 4 presents the influence of these concentrated lateral inflows on the energy losses at the singularity of energy losses at the junction boxes.

1.5 Reasons for Discussing Geometric and Hydraulic Parameters in a Separate Hydrology Paper

Apart from the use of the complete quasi-linear hyperbolic partial differential equations of gradually varied free-surface unsteady flow, with their derivation and discussion given in Chapter 3, Part I, Hydrology Paper No. 43, it was considered that a reliable estimate of geometric and hydraulic parameters that define coefficients of partial differential equations was necessary. The better these estimates and evaluations are, the better the correlation is between analytical waves (numerically integrated) and physical waves (observed on the experimental facilities).

This study is basically concerned with the accuracies attainable in using the most accurate parameters in flood routing through storm drains. Thus, the evaluation of all coefficients in partial differential equations is of a crucial importance. The writers of this paper consider a separate paper on this evaluation justified. The material presented shows the accuracy attained for these parameters. Further improvements in evaluating the parameters of boundary conditions are recommended.

Chapter 2

GEOMETRIC RELATIONS FOR THE CIRCULAR EXPERIMENTAL CONDUIT

Geometric irregularity errors, which are a function of depth of flow in the conduit, and errors made in measuring this depth of flow influence the predictions of flow characteristics in an open channel. The following is an evaluation of these errors and their relative significance.

2.1 Characteristics of a Circular Cross Section

As shown in Fig. 2.1, the geometric parameters of a circular cross section which influence the flow of a free-surface liquid are defined as follows

1 - Diameter, D
2 - Depth, y
3 - Central angle, θ
4 - Wetted perimeter, P
5 - Surface width, B
6 - Area, A.

Derived parameters of significance are:

1 - Hydraulic depth, $y_* = \frac{A}{B}$

2 - Hydraulic radius, $R = \frac{A}{P}$

3 - Section factor from Darcy-Weisbach equation, $A = AR^{\frac{1}{2}}$.

Each of these parameters may be expressed as the ratio of its value at a specific depth to its value at the upper limit of depth which is the diameter of the conduit. Figure 2.2 displays these variations as a function of the depth-diameter ratio. It is interesting to note that the hydraulic radius and the section factor maximize at values greater than one, their ratios at full section values. This infers that theoretical maximum discharge would occur at less than full depth for the same energy slope. The usual theory, based on atmospheric pressure at the free surface, does not, in practice, necessarily apply at this depth; hence, prediction of flow at depth ratios near one must be based on additional considerations.

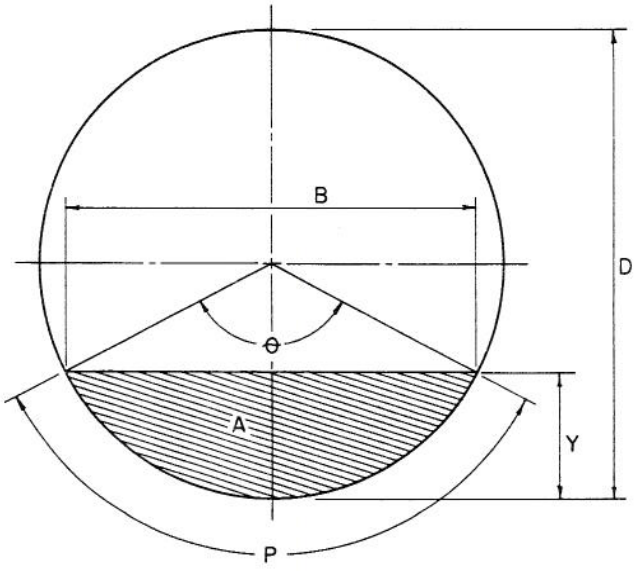

Fig. 2.1. Definition sketch for parameters of a circular cross section.

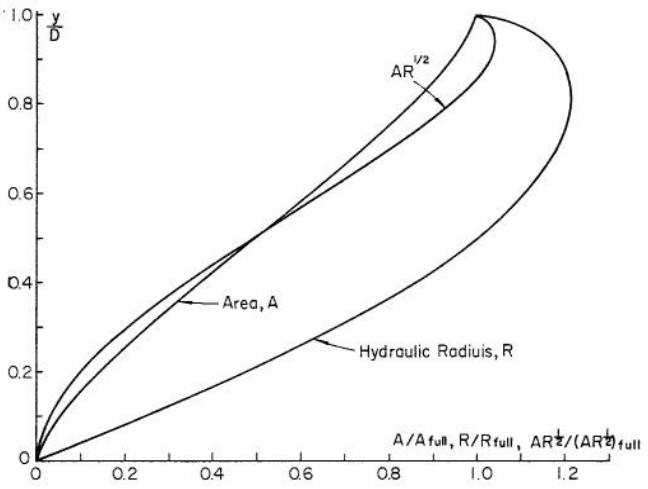

Fig. 2.2. Relative geometry of the circular cross section as it varies with relative depth.

2.2 Errors in Parameters as a Function of Errors in Depth

The relative error in each of the dependent parameters is expressed in terms of the relative error in the depth as follows:

1. Wetted perimeter defined as

$$P = \frac{D}{2}\ \theta \tag{2.1}$$

has the relative error

$$\frac{dP}{P} = \frac{d\theta}{\theta} \tag{2.2}$$

in which

$$\theta = 2\cos^{-1}\left(1 - \frac{2y}{D}\right) \tag{2.3}$$

and

$$\frac{d\theta}{\theta} = \frac{1}{\left(\frac{D}{y} - 1\right)^{\frac{1}{2}} \cos^{-1}\left(1 - \frac{2y}{D}\right)} \left(\frac{dy}{y}\right) . \tag{2.4}$$

2. Surface width defined as

$$B = D \sin\frac{\theta}{2} \tag{2.5}$$

gives

$$\frac{dB}{B} = \frac{1}{\left(\frac{D}{y} - 1\right)^{\frac{1}{2}} \tan\frac{\theta}{2}} \left[\frac{dy}{y}\right] \tag{2.6}$$

3. Area defined as

$$A = \frac{D^2}{8}(\theta - \sin\theta) \tag{2.7}$$

gives

$$\frac{dA}{A} = \frac{1 - \cos\theta}{1 - \frac{\sin\theta}{\theta}} \left(\frac{d\theta}{\theta}\right) \quad . \tag{2.8}$$

4. Hydraulic depth defined as

$$y_* = \frac{A}{B} \tag{2.9}$$

gives

$$\frac{dy_*}{y_*} = \frac{dA}{A} - \frac{dB}{B} \quad . \tag{2.10}$$

5. Hydraulic radius defined as

$$R = \frac{A}{P} \tag{2.11}$$

gives

$$\frac{dR}{R} = \frac{dA}{A} - \frac{dP}{P} \quad . \tag{2.12}$$

6. Section factor defined as

$$Z = AR^{\frac{1}{2}} \tag{2.13}$$

gives

$$\frac{dZ}{Z} = \frac{dA}{A} + \frac{dR}{2R} \quad . \tag{2.14}$$

These relative errors, (Eqs. 2.2, 2.4, 2.6, 2.8, 2.10, 2.12, and 2.14) being functions of depth, are plotted as ratios of the relative-depth error in Fig. 2.3. It may be seen that the relative error in all parameters except for that of wetted perimenter and hydraulic depth become less as depth increases for a given relative depth error. The significance of these curves will be demonstrated in the calculation of friction factors and Reynolds number.

2.3 Errors in Parameters as a Function of Ellipticity

Since no physical "circular" conduit has a mathematically circular shape, it is necessary to determine the effects of the physical variables. As a systematic approximation, an elliptical shape was assumed. Parameters describing the departure from the flow area in a circular cross section are then the eccentricity and the direction of the principal axes. The eccentricity is defined as

$$e = \sqrt{1 - \left(\frac{b}{a}\right)^2} \quad , \tag{2.15}$$

in which a and b are the major and minor semi-diameter, respectively. The direction of the principal axes, defined as the angle α is the angle that the minor axis makes with the vertical as shown in Fig. 2.4.

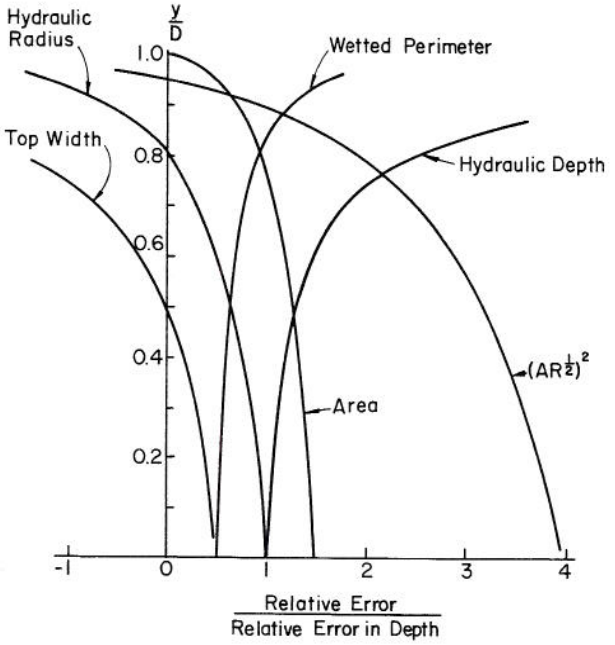

Fig. 2.3. Geometry of circular cross section represented as relative error in parameter versus relative error in depth.

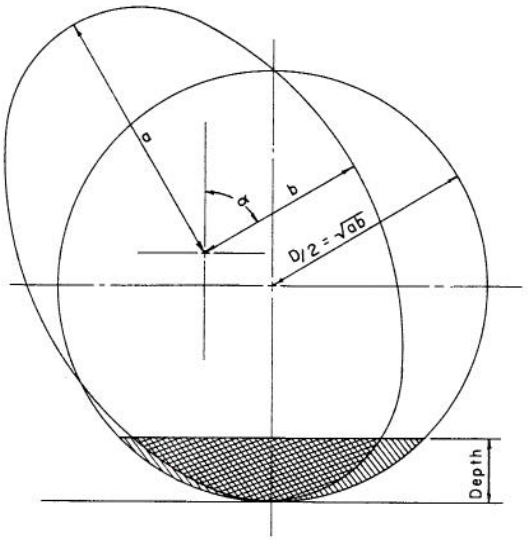

ACS – CIRCULAR SEGMENT – AES – ELLIPTIC SEGEMENT –

$\%\ \text{DIFF.} = \frac{ACS - AES}{ACS} \times 100$ $\qquad e = \sqrt{1 - \left(\frac{a}{b}\right)^2}$

Fig. 2.4. Definition sketch for the relation of circular and elliptical cross sections.

To compare circular with elliptical segments the percent of difference between the two segments was computed for depths from the bottom up to the center of the ellipse. Eccentricity was varied in increments of 0.05 up to 0.30 and for values of α ranging from 0 to $\pi/2$ in increments of $\pi/10$. For all eccentricities, the area of the complete ellipse was made equal to that for the complete circle. Depth was relative to the center of the ellipse. The results of these calculations are shown in Fig. 2.5.

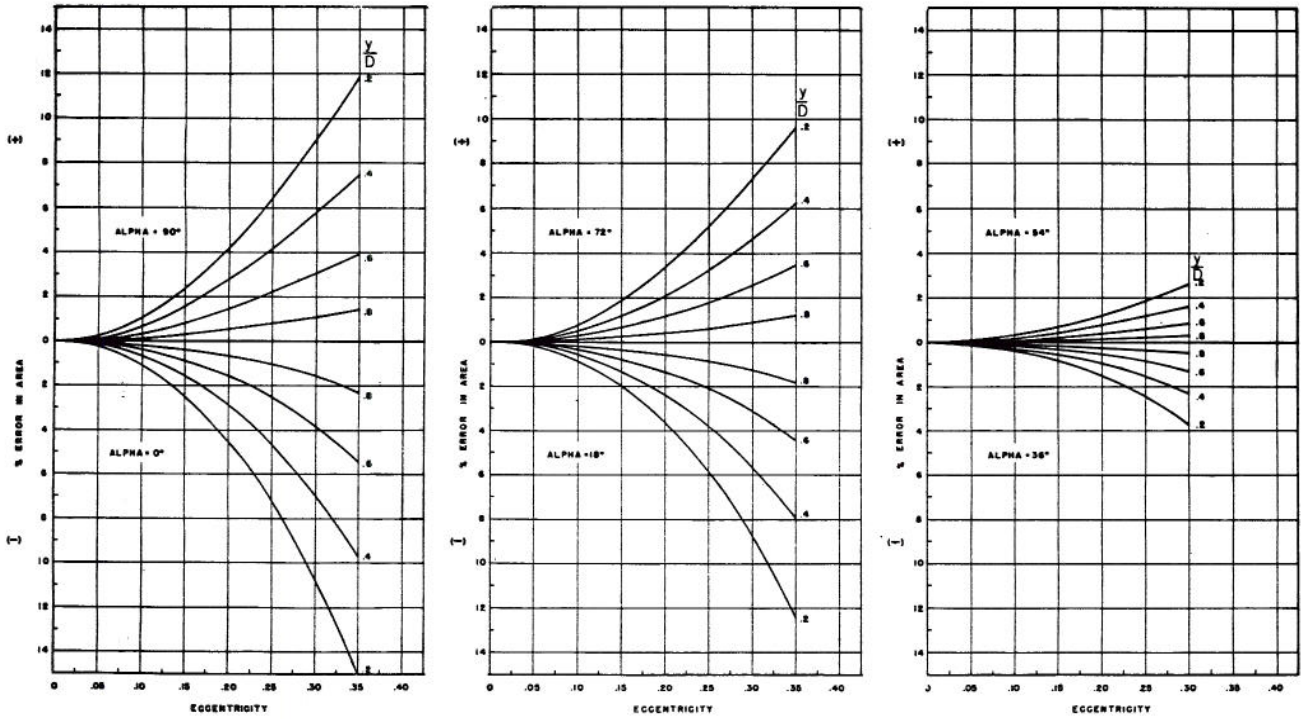

Fig. 2.5. Percent difference in area versus eccentricity and depth.

These calculations indicate

(a) that the relative error in area increases with increased eccentricity;
(b) that the relative error in area decreases with increasing depth; and
(c) that the relative error in area is maximum at the vertical and horizontal positions of the principal axes and is minimum at an angular position of 45^{o} with the horizontal.

2.4 Physical Characteristics of the Conduit

The steel pipe used as the open channel in this study had a 3 foot outside diameter, and was made of 1/2-inch thick rolled plate with a longitudinally welded joint. The 20 foot sections were butt-welded together and supported on steel rails 20 feet apart (not necessarily at the pipe joints). The total length of the pipe was approximately 822 feet. Because of the manufacturing process, handling, field welding, and the method of support it was not expected that this conduit would be perfectly circular or possess a straight line invert profile.

Measurements to the nearest 0.001 inch were made of the inside diameter of the pipe at 60^{o} intervals. These measurements were made at cross sections spaced 40 feet apart before the inside of the conduit was painted; similar measurements were made at intervals of 20 feet after the inside of the conduit was painted. An ellipse was fitted to the three measured diameters at each section and its orientation determined.

The results of the above calculations are presented in Table 2.1. The differences between the means of each of the parameters for the two surveys are not significant on the 5 percent level. This indicates that (1) the painting of the conduit had no effect to its internal geometry and (2) doubling the number of stations did not significantly improve knowledge about the geometry of the conduit.

Accepting an average area of 968.41 square inches (6.725 square feet) the mean diameter of the conduit is 2.9262 feet. This figure was used for the conduit diameter in all calculations.

TABLE 2.1. Geometry of the experimental conduit

	Number of Stations	Maximum	Mean	Minimum	Standard Deviation
Major Axis Inches	21	17.869	17.617	17.538	0.175
	41	17.913*	17.604	17.554	0.047
Minor Axis Inches	21	17.626	17.516	17.435	0.0375
	41	17.680	17.510	17.430	0.031
Eccentricity	21	0.176	0.1021	0.046	0.0310
	41	0.175	0.0993	0.051	0.0244
Alpha α Degrees	21	165.58	84.84	13.71	46.5
	41	160.37	82.94	7.78	49.43
Area $Inches^2$	21	989.5	969.47	965.3	3.84
	41	994.9*	968.4	964.1*	3.94
Wetted Perimeter Inches	21	111.51	110.373	110.13	0.2769
	41	111.82*	110.314	110.07*	0.2167
Hydraulic Radius Inches	21	8.87	8.7785	8.76	0.0183
	41	8.89	8.7742	8.75*	0.0181

*occurred at same section.
The first line of figures refers to unpainted interior of the conduit, while the second refers to the painted conduit

Eccentricity and the angle α in the observed geometry of the conduit were used to estimate possible errors in the hydraulic calculations. The percent difference between the circular and elliptical segments for the maximum and mean eccentricity at a depth ratio of 0.2 was determined (Fig. 2.5) and plotted as a function of the angle α (Fig. 2.6).

As may be seen from this plot, the error in area is maximum at an angular position of zero and 90 degrees. The maximum error for the mean eccentricity of the conduit with this depth ratio is 1.1 percent. For a mean α-angle of about 85 degrees, the maximum error for the mean eccentricity is approximately 1 percent.

For depth ratios greater than 0.2 the relative errors are less than the errors with smaller ratios. For larger eccentricities, relative errors become larger at an increasing rate. For smaller α-angles relative errors decrease to zero at approximately 45 degrees and with an absolute value which is equal to the maximum at zero degrees.

Because of the interrelated effects of depth, eccentricity and α, it appears that an error in the computation of the flow area by assuming a circular cross section instead of an approximated ellipse, may range from zero to 3 percent with 1 percent being representative.

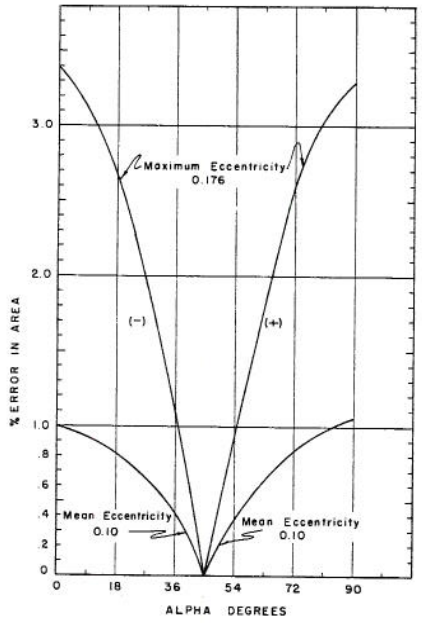

Fig. 2.6. Percent error in area at depth 0.2D, for the experimental conduit.

2.5 Errors Due to Vertical Displacements of a Circular Cross Section

Definition of Errors. The deviations of a given solid boundary from a mathematically straight alignment may be identified in three broad regions:

(a) The boundary irregularities which contribute directly to viscous shear and consequent hydraulic roughness.

(b) Misalignments of the mean boundary which occur gradually when the length of the boundary is appreciable. The misalignments are unintentional but unavoidable in a physical situation.

(c) Intentional changes in boundary direction to alter the direction of flow.

The effects of boundary irregularities and intentional boundary realignments on surface profiles, in general, are easily computed. However, the gradual boundary misalignments are generally ignored or assumed to have a negligible effect on the surface profile. Based on the energy conversions relating to such changes in cross sectional area, the foregoing assumptions may be justified; energy transfers are small, by definition, and may well be masked by the uncertainty of the mean turbulent energy loss as well as the time variable. Thus, depths computed from any commonly used formula represent only the time-distance mean values.

The following analysis was made to estimate the effect of vertical misalignments of the channel section on the elevations of the water surface.

Theory. It was expected that gradual vertical misalignments of an open-channel boundary will cause a change in surface profile. This effect may be idealized and subsequently quantitized by considering a sinusoidal channel-bottom profile [1] (see Fig. 2.7).

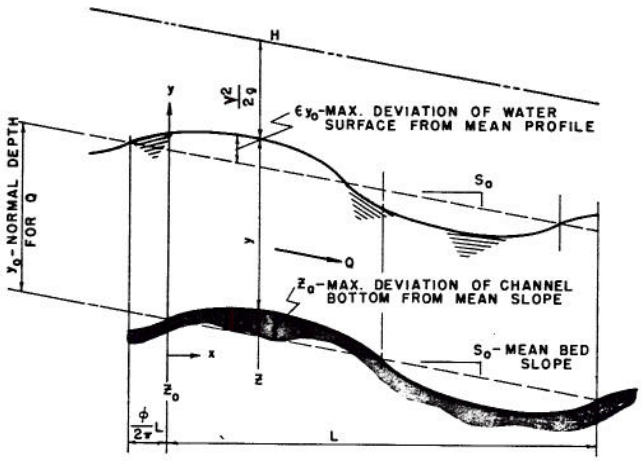

Fig. 2.7. Definition sketch of the effect of bottom irregularities.

At any section the total energy is

$$E = z + y + \frac{V^2}{2g} .$$

Upon differentiation,

$$\frac{dE}{dx} = \frac{dz}{dx} + \frac{dy}{dx} + \frac{V}{g}\frac{dV}{dx} ,$$

or

$$-S_f = S_b + \frac{dy}{dx} + \frac{V}{g}\frac{dV}{dx} , \qquad (2.16)$$

in which S_f is the rate of energy loss which may be represented by

$$S_f = \frac{f}{8g}\frac{V^2}{R} = \frac{f}{8g}\frac{Q^2}{A^2R} = \left(\frac{A_o}{A}\right)^2 \left(\frac{R_o}{R}\right) S_o \quad . \qquad (2.17)$$

The derivatives of Eq. 2.16 may be expressed as

$$z = z_o - x\,S_o + z_a \sin \frac{2\pi x}{L}$$

$$-S_b = \frac{dz}{dx} = -S_o + \frac{2\pi}{L} z_a \cos \frac{2\pi x}{L} \qquad (2.18)$$

and

$$\frac{V}{g}\frac{dV}{dx} = -\frac{Q^2 B}{gA^3}\frac{dy}{dx} = -F^2\frac{dy}{dx}$$

$$= -F^2 \left(\frac{A_o}{A}\right)^2 \left(\frac{B}{B_o}\right)\frac{dy}{dx} \quad , \qquad (2.19)$$

in which F is the Froude Number corresponding to a uniform slope S_o.

After substitution of Eqs. 2.17, 2.18 and 2.19 into Eq. 2.16 and solving for dy/dx, then

$$\frac{dy}{dx} = \frac{1}{1 - F^2\left(\frac{A_o}{A}\right)^2\left(\frac{B}{B_o}\right)} S_o \left\{\left[1 - \left(\frac{A_o}{A}\right)^2\left(\frac{R_o}{R}\right)\right] - \frac{2\pi z_a}{L}\cos\frac{2\pi x}{L}\right\} \quad . \qquad (2.20)$$

Equation 2.20 is the differential equation of the depth resulting from a sinusoidally-varying bottom of amplitude z_a in length L. A solution to this equation may be found if the geometry ratios can be expressed in terms of the depth ratios (y/y_o). It is not possible to express the geometry of a circular section as a simple continuous function of the depth-normal depth ratio. It is possible, however, to achieve a solution if the depth ratio is assumed to be

$$\frac{y}{y_o} = 1 + \varepsilon \sin\left(\frac{2\pi x}{L} - \phi\right) \quad , \qquad (2.21)$$

in which ε is the ratio of amplitude to y_o, and ϕ is the phase angle for the depth wave. If this is done then

$$\frac{dy}{dx} = \frac{2\pi y_o}{L}\,\varepsilon \cos\left(\frac{2\pi x}{L} - \phi\right) \quad . \qquad (2.22)$$

From Eqs. 2.20 and 2.22, expanding the cosine of the sum and equating the coefficients of the unknown phase angle ϕ in Eqs. 2.20 and 2.22, the value of ϕ is determined for the infinite wide channel to be

$$\phi = \tan^{-1}\left[\frac{-3\,S_o\,L}{2\pi y_o(1 - F^2)}\right] \quad . \qquad (2.23)$$

The amplitude of the depth wave y_o can now be evaluated from

$$\varepsilon = -\frac{2\pi z_a \sin\phi}{3\,S_o\,L} \quad . \qquad (2.24)$$

Equations 2.23 and 2.24, for the infinite wide channels, relate those quantities which are required to estimate the effect which the periodic channel irregularities have on the corresponding changes in the depth of flow. This is an approximate evaluation of effects of periodic bottom irregularities in conduits.

Calculations and results. Equations 2.23 and 2.24 were solved for various combinations of

(a) channel slope,
(b) wave length of channel irregularity,
(c) amplitude of channel irregularity, and
(d) normal depth.

The Darcy-Weisbach friction factor was taken as a constant 0.012.

Table 2.2 presents the results of these calculations. The results indicate, as expected, that for a Froude number greater than one the depth wave is nearly in phase with the bottom wave. The slight difference is due to flow resistance. For a Froude number less than one the depth wave is out of phase with the bottom wave by essentially π. Again, the slight difference is due to flow resistance.

Note that the amplitude of the depth wave is unchanged for various lengths of the bottom wave, provided that other parameters are also unchanged. The amplitude of the depth wave compared to the length of the bottom wave ranges from approximately one for low Froude numbers to approximately three for Froude numbers close to one.

Significance to physical observations. The channel invert was aligned as carefully as possible to a constant, uniform slope. All leveling was done with a self-leveling level with an optical micrometer which could measure to at least 0.001 inch. Alignment was accomplished by first adjusting the conduit to a predetermined position on the supporting rails. Then the invert elevations were observed at 45 positions approximately 20 feet apart and least-square determination of the slope and the deviations at each position was made. If the deviations showed a consistent or excessive trend in a given length, that portion of the conduit was readjusted and the elevations redetermined.

Due to unavoidable irregularities in successive sections of the conduit and the method of joining sections, it was impossible to completely eliminate all deviations from the mean slope. Table 2.3 presents the results of mean slope determinations and the corresponding maximum and root-mean-square deviations from the slope of least-square fit.

These results show that the invert profile of the conduit had an undulating bottom with approximately 0.01 foot of amplitude and 20 to 40 feet of wave length.

Equations 2.23 and 2.24 were solved using the case of an infinitely wide channel with sinusoidal bottom. This case may be considered as the limiting one for a circular cross section flowing partially full if the radius is considered to remain constant and the centerline of the section to vary sinusoidally about the mean slope. Thus, the entire section may

be considered as changing position vertically rather than only a sinusoidal change of the invert or radius.

On consideration of the results of Table 2.2 in predicting the effect on the observed water surface profile, it may be concluded that for the slopes used in this study the observed depths may deviate from the ideal by 0.01 to 0.03 of a foot on the average. Based on the maximum deviations the water depth may differ from the ideal by 0.03 to 0.09 of a foot.

TABLE 2.2. Theoretical effect of bottom irregularity on water surface profiles.

Slope	Froude No.	z_a-ft.	L-ft.	ϕ-Rad.	εy_o-ft.	Slope	Froude No.	z_a-ft.	L-ft.	ϕ-Rad.	εy_o-ft.
.0100	2.582	.01	20	6.266	.002			.03	20	3.170	.090
			40	6.249	.002				40	3.198	.090
			60	6.232	.002				60	3.227	.090
			80	6.216	.002				80	3.255	.090
		.02	20	6.266	.004			.04	20	3.170	.120
			40	6.249	.004				40	3.198	.120
			60	6.232	.004				60	3.227	.120
			80	6.216	.004				80	3.255	.120
		.03	20	6.266	.005	.0001	.258	.01	20	3.142	.011
			40	6.249	.005				40	3.143	.011
			60	6.232	.005				60	3.144	.011
			80	6.216	.005				80	3.145	.011
		.04	20	6.266	.007			.02	20	3.142	.021
			40	6.249	.007				40	3.143	.021
			60	6.232	.007				60	3.144	.021
			80	6.216	.007				80	3.145	.021
.001	.816	.01	20	3.170	.030			.03	20	3.142	.032
			40	3.198	.030				40	3.143	.032
			60	3.227	.030				60	3.144	.032
			80	3.255	.030				80	3.145	.032
		.02	20	3.170	.060			.04	20	3.142	.043
			40	3.198	.060				40	3.143	.043
			60	3.277	.060				60	3.144	.043
			80	3.255	.060				80	3.145	.043

TABLE 2.3. Slope deviations of the experimental conduit

Slope	Max. Deviation, ft	Root-Mean-Square Deviation, ft
.0000052	+.0188	.0116
.0000157	+.0182	.0135
.0000303	+.0214	.0099
.0001325	+.0195	.0099
.0005197	+.0347	.0117
.0010101	+.0279	.0119
.0074578	-.0240	.0133
.0200690	+.0375	.0141

Chapter 3

HYDRAULIC RESISTANCE OF THE EXPERIMENTAL CONDUIT

3.1 Expressions for the Friction Factor of Partly Flowing Conduits

Resistance to motion of open-channel flow, including the free-surface flow in conduits, due to boundary roughness can be expressed in various forms. Foremost among those commonly in use are the Chézy, Manning, Colebrook-White, Hazen-Williams, and Darcy-Weisbach equations of flow resistance.

The Committee for Hydromechanics of the Hydraulics Division of the American Society of Civil Engineers [2] recommended the use of the Darcy-Weisbach equation for future presentation of resistance data in pipes. Thus, boundary resistance in conduits is evaluated and expressed in this study in terms of the Darcy-Weisbach equation

$$S_f = \frac{f}{D} \cdot \frac{V^2}{2g} \quad , \tag{3.1}$$

in which S_f is the slope of the energy gradient, f is the Darcy-Weisbach friction factor, V is the mean flow velocity, and D is the diameter of the conduits flowing full. For channel cross sections other than circular, and for partly full circular conduits, the diameter (D) is customarily replaced by four times the hydraulic radius $(4R)$. The validity of this replacement may be questioned for open-channel flow and for partly full circular conduits. However, for lack of a better length parameter describing the velocity gradients of the velocity distribution in a cross section, and hence the shear stresses, the hydraulic radius is commonly used. Equation 3.1 thus becomes

$$S_f = \frac{f}{R} \cdot \frac{V^2}{8g} \quad , \tag{3.2}$$

in which the hydraulic radius (R) is defined as the cross sectional area divided by the wetted perimeter (P), or $R = A/P$.

It has been demonstrated that the Darcy-Weisbach friction factor f is a function of the Reynolds number, the relative roughness (k/y), and the channel cross sectional shape, in which k is the absolute boundary roughness, y is the depth of flow, and k/y is the relative roughness. The form of this theoretical relation depends in turn on the range of the Reynolds number, the relative roughness, and the shape of the channel cross section. For hydraulically smooth boundaries, such as the boundary of experimental conduit used in this study, and for Reynolds number greater than 2.5×10^4, the Prandtl-von Karman equation [4]

$$\frac{1}{\sqrt{f}} = a \log_{10} (R_e \sqrt{f}) + b \tag{3.3}$$

relates the friction factor f only in terms of the Reynolds number (R_e). The constants a and b in Eq. 3.3 are determined experimentally. Their values depend on the selection of the Reynolds number length parameter, assuming that the mean flow velocity and the kinematic viscosity are always uniquely defined. For open channels, it is convenient to express the Reynolds number as

$$R_e = \frac{VR}{\nu} \quad , \tag{3.4}$$

in which R is the hydraulic radius of the given cross section. Equation 3.3 for open channels with smooth boundaries becomes

$$\frac{1}{\sqrt{f}} = 2 \log_{10} (R_e \sqrt{f}) + 0.4 \quad . \tag{3.5}$$

In the case of full flow through a circular cross section, the length parameter in the Reynolds number is the diameter, or $R_e^* = VD/\nu$. In this case Eq. 3.3 takes the familiar form

$$\frac{1}{\sqrt{f}} = 2 \log_{10} (R_e^* \sqrt{f}) - 0.8 \quad . \tag{3.6}$$

The evaluation of f from Eq. 3.3 for a given R_e requires an iterative procedure, and often excessive computations are needed. To simplify computations (within practical limits of Reynolds numbers for specific conditions) it is convenient to use a simplified form of the f to R_e relation. Thus, a practical form of expression for this relation is

$$f = c R_e^d \quad , \tag{3.7}$$

in which c and d are constants to be empirically determined.

The purposes of the experimental investigations of hydraulic resistance in this study were: (a) to confirm the hydraulically-smooth surfaces of the experimental conduit; (b) to develop a simplified expression for the friction factor as it is related to Reynolds number, in the form of Eq. 3.7, and (c) to determine the effects of an assumed constant friction factor on unsteady flow through storm drains and compare these with the effects of a changing friction factor related to Reynolds number in the same type of flow.

3.2 Observations on Hydraulic Resistance in the Experimental Conduit

The experimental conduit and the instrumentation used are described in Part II (Hydrology Paper No. 44) of these series of four papers on flood routing through storm drains. A brief summary is repeated in this subchapter.

The experimental facilities consisted of a 3-foot diameter, 822-foot long circular conduit with a slope adjustable between 0 and approximately 4 percent. Water surface elevations used to study hydraulic resistance are measured by hook gages

located at 16 positions along the conduit (see Table 5.1, Hydrology Paper No. 44). The invert slope of the conduit was carefully determined by means of a precise self-leveling level with an optical micrometer. Discharge for a desired depth of flow in the conduit was estimated from previous observations (see Table 5.3 Hydrology Paper No. 44) and established at the conduit inlet. The downstream outflow-control gate was adjusted to produce the desired backwater or drawdown curve. Several conditions of non-uniform flow were established, both above and below normal depth. Hook gage levels at the various piezometer locations were read at approximately 15 minute intervals until the readings stabilized. Hook gage readings, gage zeros, and invert elevations were transferred to punch cards along with the steady discharge rate and the conduit slope. Data was then analyzed by means of a digital computer.

3.3 Analysis of Experimental Results

The total energy per unit weight flowing in a partially full channel is defined as: total energy head = invert elevation + depth of flow + velocity head. The difference in successive values of total energy head divided by the distance between conduit stations represents the rate of energy loss. This loss rate $(E_2-E_1)/\Delta x$, the average hydraulic radius, and the average of the velocity heads at the ends of the reach, $(V^2/2g)_{av}$, were then substituted into the resistance equation to evaluate the friction factor f as

$$f = \frac{4R_{av}}{(V^2/2g)_{av}} \cdot \frac{E_2-E_1}{\Delta x} \quad . \tag{3.8}$$

The Darcy-Weisbach friction factor f was computed initially by considering the slope of the energy gradient between the successive piezometer locations. This approach gave a large number of less accurately determined friction factors. The computations were performed by the digital computer thus eliminating any subjective bias in establishing the slope of the gradient at these short distances. A plot of these f - values versus Reynolds number, however, resulted in a wide scatter of values as shown in Fig. 3.1. As expected, this was largely due to experimental errors in observation of depth, the influence of unavoidable bottom irregularities on the surface water profile, and small surface waves and pulsations, which produced substantial variation in the slopes of the energy gradient computed from the short lengths of conduit. The use of small reaches in computing the slope and other parameters of Eq. 3.8, therefore, resulted in a large scatter of points in Fig. 3.1 around the expected smooth curve.

It was apparent that the mean slope of a long reach was necessary to define the friction factor more accurately. Therefore, the values of energy heads at the piezometer locations throughout the conduit were plotted and the best estimate of the average slope was graphically determined. The least square fit of these

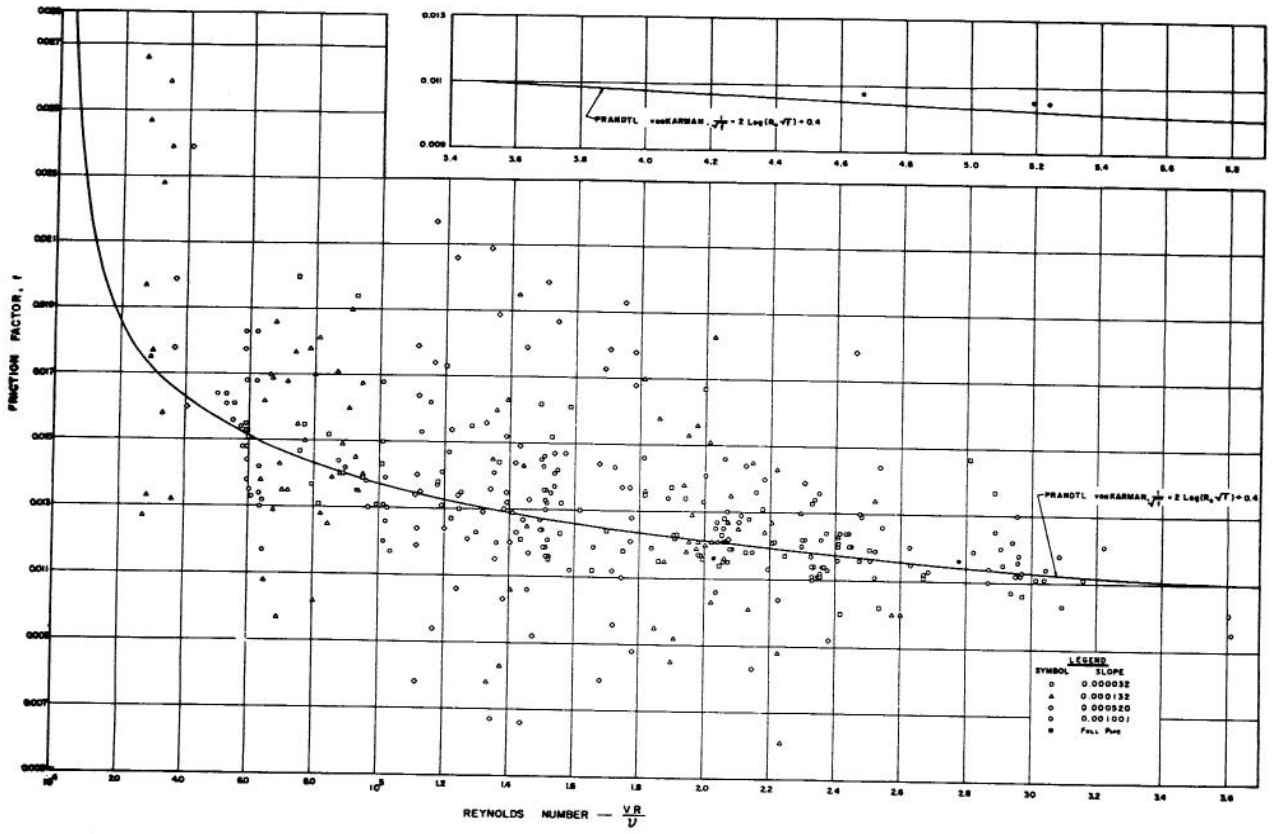

Fig. 3.1. Variation of Darcy-Weisbach friction factor f with Reynolds number R_e (computed from small reaches of the conduit).

data was not used because it would not produce the expected results in regions of high curvature of the water surface the slope of the energy gradient did not remain constant. This variation occurs because friction factor varies with Reynolds number and thus with depth. The graphically-fitted average slope of the energy gradient was taken to be the most representative slope of the particular flow conditions.

The following procedure was used to determine the average value of the hydraulic radius and the average velocity head. The depths of flow at both ends of the reach were computed based on the energy heads indicated by the uniform gradient. These two depths were then averaged and from this value the average area, average hydraulic radius, average velocity, and average velocity head were computed.

Even with these precautions and averagings, as it was expected, a scattering of points (f, R_e) remained but with much smaller deviations than in Fig. 3.1. The results of these averaging computations for the entire length of conduit are presented in Fig. 3.2. It is apparent that the points computed from the average slopes of the energy line show an improved relation of the friction factor with the Reynolds number. The points tend to cluster around the Prandtl-von Karman smooth-boundary friction-factor equation.

The plotted points represent the results in a range of depth from 0.56 to 2.6 feet, or depth-to-diameter ratios of 0.19 to 0.89. The discharges varied from 2.25 to 72.0 cfs. The corresponding Reynolds-number range is from approximately 3×10^4 to 1×10^6.

For the data shown in Fig. 3.2, the values of the constants a and b in Eq. 3.3 are 2.075 and 0.1434, respectively. These will be compared later with the constants of 2.0 and 0.4 in the Prandtl-von Karman equation for the free-surface smooth boundary flow. For the values $a = 2.075$ and $b = 0.1434$ in Eq. 3.3 the mean absolute deviation of the points in Fig. 3.2 from the line defined by Eq. 2.3 is 0.00167, with a standard deviation of 0.0024. The two extremely departing points on the right side of Fig. 3.2 make the standard deviation greater than it really should be.

The two points in Fig. 3.2, which are much above the other points and the curve of the Prandtl-von Karman equation could not be verified as inaccuracy of observations or the ensuing data processing. It is considered to be reasonable to assume that they are mistakes either in observations or in data processing, their values being about two times the expected values on both the Prandtl-von Karman curve for their corresponding Reynolds numbers and the expected values determined from the curve fitted to all observational points. These two points are retained in Fig. 3.2 to show that mistakes are often unavoidable in experimental results, and that they should not be arbitrarily removed.

To save computing time, the constants c and d in Eq. 3.7 were evaluated and used in subsequent computer programs. The constants c and d in Eq. 3.7 used for integrating unsteady-flow equations, are estimated from data in Fig. 3.2 to be 0.10939 and -0.17944, respectively.

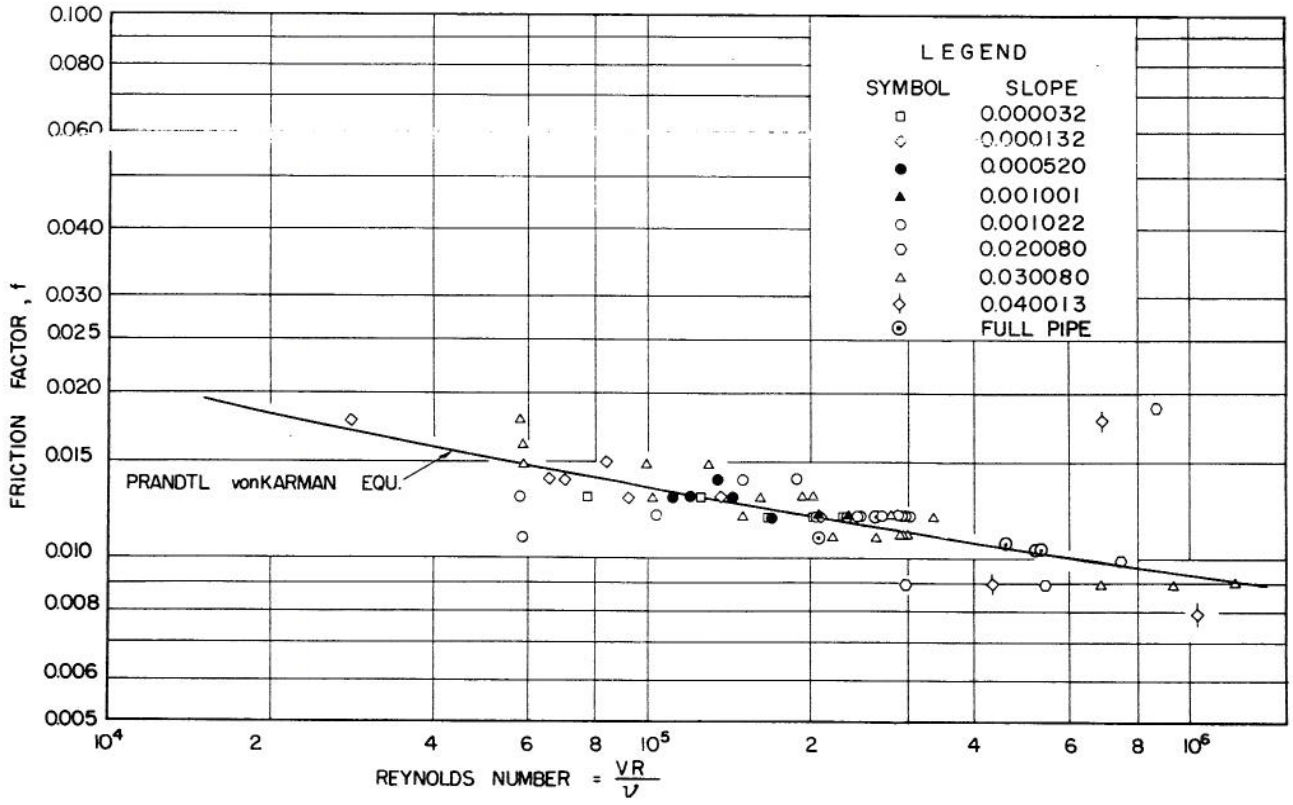

Fig. 3.2. Variation of Darcy-Weisbach friction factor f with Reynolds number R_e based on the slope representative of the entire length of experimental conduit.

Although Eqs. 3.3 and 3.7 show a decrease of f with an increase of R_e it can be shown that for a limited range of R_e the changing friction factor f may be replaced by an average value or a representative constant. An investigation, presented in Part I (Hydrology Paper No. 43), was done for the range of R_e-values observed in this study and shows a relatively small difference between the analytical waves computed by the use of the friction factor in Eq. 3.7 and by the use of a constant representative friction factor f_c.

3.4 Effect of Depth on Friction Factor

The Darcy-Weisbach friction factor, f, has been demonstrated to be a function of Reynolds number. Although it is not possible to separate the effects of velocity and geometry on the friction factor, there have been attempts in the past [3] to demonstrate the effect of depth alone on friction factor. A similar attempt was made in this study to compare results with previously published results.

The Darcy-Weisbach equation relates friction factor, depth, velocity, and slope of energy line in the general form

$$F_1(f, y, V, S_f) = 0 \quad . \tag{3.9}$$

The Prandtl-von Karman equation relates the friction factor, depth, velocity, and properties of the fluid in the form

$$F_2(f, y, V, \nu) = 0 \quad . \tag{3.10}$$

By eliminating the velocity V between Eqs. 3.9 and 3.10, the new general function is

$$F_3(f, y, S_f, \nu) = 0 \quad , \tag{3.11}$$

so that for a given slope (S_f), a kinematic viscosity (ν), and a depth of flow (y) the friction factor (f) may be computed. Because S_f is a function of f for this analysis of the long conduit the slope of energy line is assumed to be equal to the bottom slope, or $S_f = S_o$.

Equation 3.2 gives

$$V = \left(\frac{8gS_fR}{f}\right)^{1/2} \quad , \tag{3.12}$$

so that the Prandtl-von Karman equation becomes now in substituting Eq. 3.12 for V in R_e in Eq. 3.5 and for $S_f = S_o$ for the steady flow, with S_o being the bottom slope,

$$\frac{1}{\sqrt{f}} = 2 \log_{10}\left[\frac{(8gS_o)^{\frac{1}{2}}R^{3/2}}{\nu}\right] + 0.4, \tag{3.13}$$

and the fitted Eq. 3.3 with $a = 0.1434$ and $b = 2.075$ becomes

$$\frac{1}{\sqrt{f}} = 0.1434 \log_{10}\left(\frac{(8gS_o)^{\frac{1}{2}}R^{3/2}}{\nu}\right) + 2.075 \quad . \tag{3.14}$$

A plot of the results of Eqs. 3.13 and 3.14 is given in Fig. 3.3 for two extreme slopes, and these two equations are presented in the form relating the relative friction factor to the relative depth. The relative friction factor is defined as the ratio of the partial-flow Darcy-Weisbach friction factor to the full-flow friction factor of a conduit. The relative depth is defined as the ratio of the partial-flow depth to the full-flow depth (or the diameter) of a conduit.

Figure 3.3 shows that both the theoretical relation of relative friction factor to the relative depth of the Prandtl-von Karman equation, or the experimental relation obtained in this study lie appreciably below the curve proposed by Camp [3]. Figure 3.3 further shows that variations of f with depth from the curves given are equal to or lesser than the errors in the computations of f for a free-surface flow within the upper range of the conduit (upper 2/3 of the diameter). Below the lower 1/3 of the diameter an appreciable change of the friction factor occurs with a change of water depth.

3.5 Effect of Measurement Errors on Computed Friction Factors

To estimate the effect of observational errors on the computed friction factors, certain assumptions are required. For the following analysis the assumptions about the numerical values of parameters and errors are: Internal diameter of the conduit (D) is 3 feet, the depth (y) is 1.5 feet ± 0.005 foot, the bottom slope S_o is $0.001 \pm .00001$, and the discharge (Q) is 30 cubic feet per second $\pm$ 0.3 cubic foot per second. These values will be used in the expression for the friction factor

$$f = \frac{8gS_fRA^2}{Q^2} \quad . \tag{3.15}$$

with $S_f = S_o$ for the steady flow.

The errors are ± 0.005 foot, ± 0.00001, and ± 0.3 cubic foot per second respectively for y, S_f and Q. By differentiating Eq. 3.15, the error equation for the assumed independent errors in the four quantities $(y, S_f, RA^2$ and $Q)$ is

$$\varepsilon^2(f) = \left[\frac{\partial f}{\partial S_f}\ \varepsilon(S_f)\right]^2 + \left[\frac{\partial f}{\partial (RA^2)}\ \varepsilon(RA^2)\right]^2 + \left[\frac{\partial f}{\partial Q}\ \varepsilon(Q)\right]^2 \quad , \tag{3.16}$$

in which $\varepsilon(f)$, $\varepsilon(S_f)$, $\varepsilon(RA^2)$, and $\varepsilon(Q)$ represent the errors in f, S_f, RA^2, and Q respectively. The error $\varepsilon(RA^2)$ is evaluated by means of Fig. 2.3 from the error in the depth (y), given as $\varepsilon(y)$. The derivatives $\partial f/\partial S_f$, $\partial f/\partial (RA^2)$ and $\partial f/\partial Q$ are computed from Eq. 3.15, and the above numerical values of parameters are used to numerically determine these derivatives in Eq. 3.16.

Assuming that the above errors in y, S_f, and Q are their respective standard deviations of random errors, then the standard error of random errors in the friction factor, $\varepsilon(f)$, is

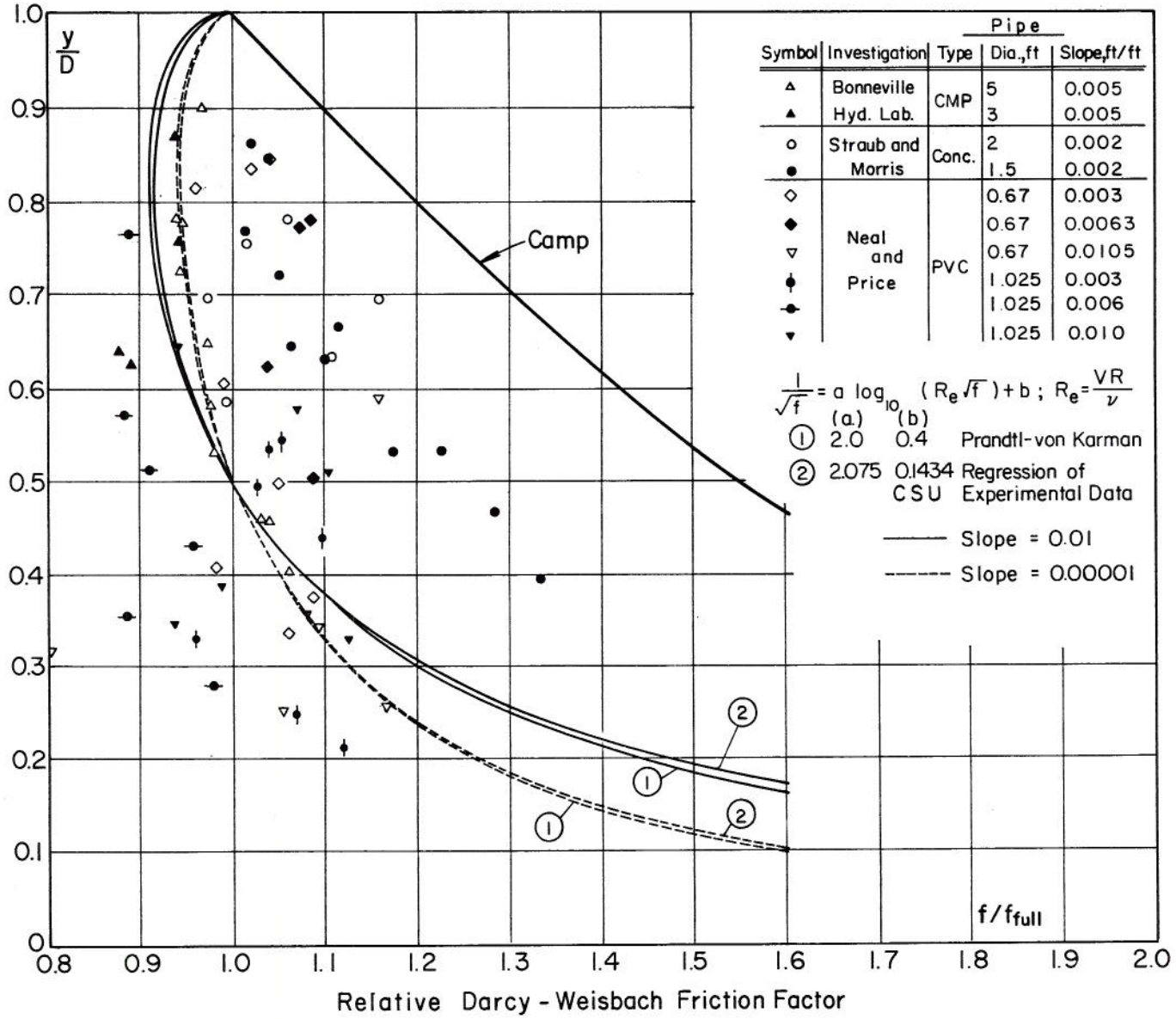

Fig. 3.3. Variation of Darcy-Weisbach friction factor f with depth of flow in a circular cross section.

$$\varepsilon(f) = \{(2.681 \times 0.00001)^2 + (0.000286 \times 0.0997)^2 + (0.0001787 \times 0.3)^2\}^{\frac{1}{2}} =$$

$$= \{7.18 \times 10^{-10} + 8.12 \times 10^{-10} + 28.5 \times 10^{-10}\}^{\frac{1}{2}} = 6.61 \times 10^{-5}$$

For the representative constant friction factor of 0.012 for this conduit and the range of Reynolds numbers used in this study, this estimated standard error of 6.61×10^{-5} represents only a 0.55 percent error.

For the above particular numerical case it is noted that the largest contribution of error to the friction factor is by the error made in discharge measurement whereas the error in slope has the least effect. The standard error in the friction factor of 6.6×10^{-5} may be considered as a lower boundary in practical evaluations of random errors.

3.6 Conclusions

From the consideration of the experimental data it can be concluded that:

(1) The boundary of the conduit used in this experimental study is hydraulically smooth.

(2) Estimations of friction factors made from comparing water elevations across short reaches result in significant random errors (shown by Fig. 3.1). By using the entire conduit length (822 feet) for computing the energy slope the spread of errors is much smaller (shown by Fig. 3.2).

(3) The friction factor may be expressed for practical applications as

$$f = 0.10939\ R_e^{-0.17944}, \qquad (3.17)$$

for a range of Reynolds numbers from 3×10^4 to 1×10^6.

(4) An average Darcy-Weisbach friction factor of 0.012 is considered representative of the smoothness of the boundary of the experimental conduit for the range of R_e in this study.

(5) Roughness values for any depth in a circular cross section can be estimated from the roughness of the full conduit (shown by Fig. 3.3)

(6) The assumption of a representative constant friction factor for CSU smooth pipe may be in error by a maximum of ±10 percent for depths in excess of one-third of the diameter shown in Fig. 3.3, lines (2), and the friction factor of a full-pipe flow is not representative of roughness for depths less than one-third full.

Chapter 4

ENERGY LOSSES AT JUNCTION BOXES

4.1 Definition of Losses at Junctions

The previous chapter considered the hydraulic energy losses resulting from the effects of the boundary roughness. This chapter considers the energy losses resulting from local changes in channel geometry and the losses accompanying energy exchange when the main flow and lateral inflows interact at junction boxes. The junction of any two storm drainage systems presents the problems of these two energy losses. The two energy losses, however, cannot be separated whenever the intersecting flows are associated with a change in boundary geometry, which is usually the case with junction boxes of storm drainage systems. Only the energy loss due to the change in boundary configuration can readily be evaluated.

The need for an experimental evaluation of these two losses at junction boxes was necessary to evaluate the validity of applying numerical solutions of unsteady flow equations along a conduit with local lateral inflow. Mathematical representation of the junction-box loss appears as a discontinuity in the application of unsteady flow equations. Thus, the junction-box loss presents a boundary condition which is satisfied by the conditions upstream and downstream of the junction box.

4.2 Brief Review of Previous Investigations of Losses at Junction Boxes

There is a limited number of references on energy losses at hydraulic junctions of various types, particularly for free-surface flow. The following brief review of several references and the material presented in this chapter are taken from the M.S thesis by William L. Lorah entitled "Free-Surface Flow Energy Losses in a 90° Junction Box", Colorado State University, June 1966, which was done under this project on "Unsteady Free-Surface Flow in a Long Storm Drain."

In 1926 Stevens [5] developed a theoretical equation from the energy equation to express impact and eddies losses at the intersection of two full-flowing pipes. His computations assumed that eddies losses for a 90° junction are equal to the upstream velocity head in the main pipe, plus the velocity head in the lateral pipe times the ratio of lateral to main flow.

Taylor [6], in 1944, derived a relation between the upstream and downstream depths at a channel junction. His derivation was based on the momentum equation and these assumptions:

(1) flow was parallel to the channel walls,
(2) velocity was uniformly distributed immediately above and below the junction, and
(3) the depths of flow entering the junction were equal. His resulting equation was

$$k_2 = \frac{\left(\frac{Q_\ell}{Q_d}\right)^2 \left[\frac{y_u}{y_d} - 1\right]}{4\left(\frac{y_u}{y_d}\right)^2 \left[2\left(\frac{Q_\ell}{Q_d}\right) - \left(\frac{Q_\ell}{Q_d}\right)^2 (1+\cos\phi)\,\frac{y_u}{y_d} - 1\right]}, \quad (4.1)$$

in which k_2 is the ratio of the velocity head to depth in the branch channel, Q_ℓ is the branch flow, Q_d is the downstream flow, y_u is the depth upstream y_d is the depth downstream, and ϕ is the angle the branch channel makes with the main channel.

He tested a model junction in which the main and branch channels were of equal width and at the same intersecting elevation. He also tested 45° and 135° junctions for combining and dividing flow. His experimental results for a 45° combining flow agreed well with his theory but there was lack of agreement between theory and model for the 135° combining flow. This disagreement was attributed to the distortion of velocity distribution below the channel junction and to the flow not being parallel to the channel walls.

In 1950 the University of Minnesota modeled open-channel junctions for a drainage system to be used at Whiting Field Naval Air Station [7]. The channels were trapezoidal, with a maximum prototype discharge of 960 cubic feet per second. Their slopes were supercritical, which normally creates hydraulic jumps in both the main and side channels. One of the conclusions of this report was that model studies of this type of junction were necessary until better design criteria could be developed.

Discussing manhole and other junction losses in storm sewer drains in 1964, Jens and McPherson [8, page 20-31] state "There are virtually no data on which estimates of such losses can be based, other than those from the recent University of Missouri experiments."

In 1958 a study of storm drain junctions [9] was conducted at the University of Missouri, It was both an analytical and experimental investigation, involving full-pipe relation only, with the top of the junction box open to the atmosphere. This work was concerned with pressure changes across the various junctions studied. The results of this study were graphic procedures for designing full-pipe storm drain junctions. These graphs represented the empirical relations between the ratio of lateral flow to the flow leaving the junction, and the ratio of pressure head lost in the junction to the velocity head of either the main or lateral flow.

Discussing the present state of knowledge concerning channel junctions, Chow [10, page 512] states "The problem is so complicated that only a few simple and specific cases have been studied. The conclusions of such studies indicate that generalization of the problem is not possible or even desirable."

4.3 Experimental Facilities

The evaluation of energy losses accompanying lateral inflow into a main conduit having free-surface flow was accomplished on two separate experimental facilities in this study. A plastic pipe with a six-inch diameter provided a means of economically developing the basic evaluations of junction box losses. The results were then verified by a limited number of tests in the 3-foot diameter conduit. Agreement between the two systems was obtained based on Froude similarity relation. The details of the two physical systems is presented in Chapter 2, Hydrology Paper No. 44.

In the model studies of the relation of power loss at the junction to other hydraulic properties only one type of junction box configuration was studied. This junction box had two lateral inlets at different elevations above the invert of the main conduit. The two lateral inlets were studied separately. The main and lateral conduits entering the junction box were circular, having diameters of 6.250 inches and 1.873 inches, respectively. The study was limited to steady, free-surface, subcritical combining flow.

The results of this study are in the form of two equations (one for each inlet) which show the relations between the power loss in the junction, the power entering the junction, the rate of main conduit flow into the junction, the rate of lateral inflow, and the depth of flow entering the junction from the main conduit.

This particular study is one of the foundations for further study of unsteady flow through a similar prototype junction box.

The experimental facilities for the six-inch pipe are described in Hydrology Paper No. 44, Chapter 2, subchapter 2.3.

Photographs of typical flow conditions are presented in Fig. 4.1, 4.2, 4.3 and 4.4. Figures 4.1 and 4.2 show the flow conditions with the lower inlet, and Figures 4.3 and 4.4 show the flow conditions with the upper inlet for the two extreme relative discharges of lateral inflow to main conduit flow (Q_r).

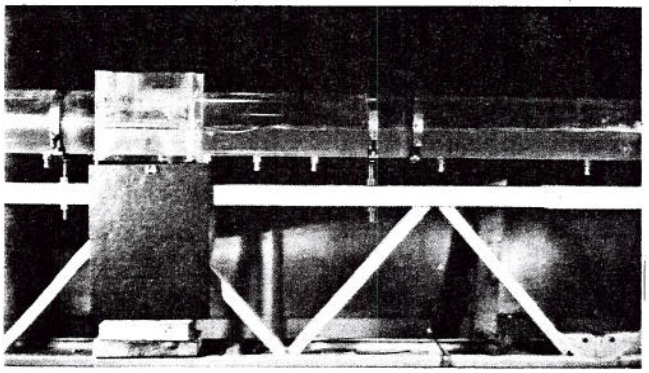

Fig. 4.1. Flow conditions for S_o = 0.000537, Q_r = 5.56 with lower inlet.

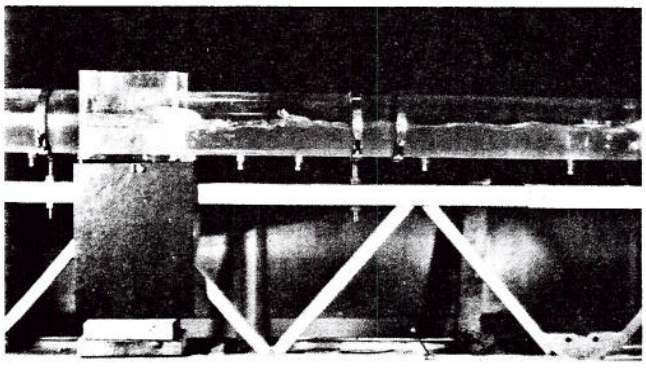

Fig. 4.2. Flow conditions for S_o = 0.000537, Q_r = 8.44 with lower inlet.

The following conditions should be noted in these photographs:

(1) The turbulence within the junction box.
(2) The drop in water depth from the upstream to the downstream side of the junction box.
(3) The persistence of turbulence, as evidenced by the entrained air and surface waves several pipe diameters downstream of the junction box.

4.4 Energy Loss Evaluations

The energy of steady, free-surface flow in any shaped channel may be defined as

$$E = z + y \cos \theta + \alpha \frac{V^2}{2g} \quad , \qquad (4.2)$$

in which E is the energy head, z is the elevation of the channel bottom above the zero datum, y is the depth of water perpendicular to the channel bottom, V is the mean velocity, α is the velocity distribution coefficient for the energy, and θ is the angle the channel bottom makes with the horizontal as shown in Fig. 4.5 for the definition of energy heads and differences. For the cases considered, θ is, within the limits of physical observation, sufficiently close to zero so that the cosine of θ is essentially one. It is also assumed that the velocity distribution coefficient α is sufficiently uniform and may safely be assumed to be one. Thus the total energy head equation may be written as

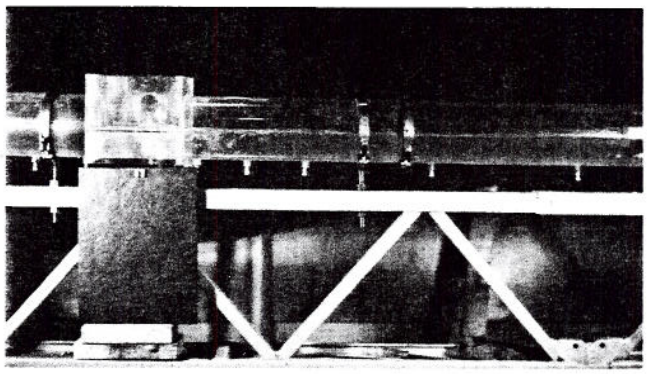

Fig. 4.3. Flow conditions for S_o = 0.000537, Q_r = 3.30 with upper inlet.

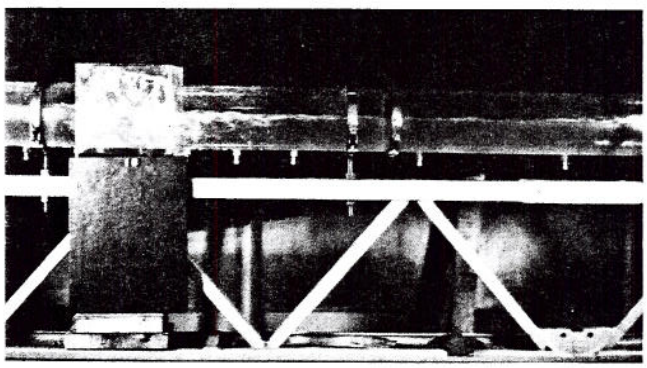

Fig. 4.4. Flow conditions for S_o = 0.000537, Q_r = 7.40 with upper inlet.

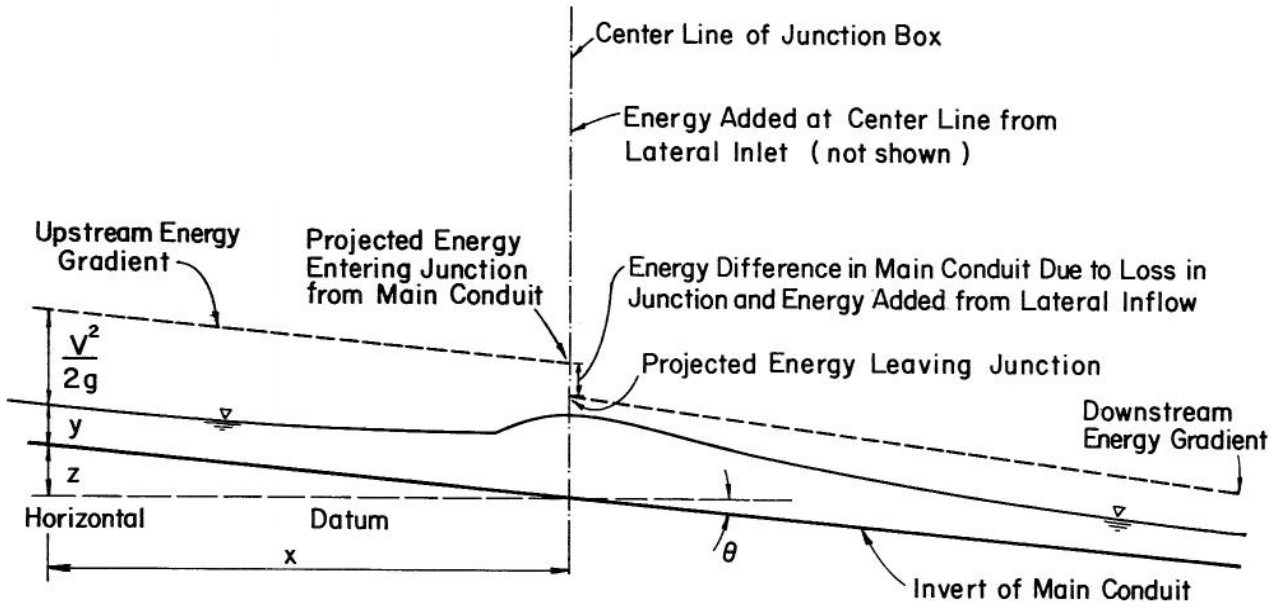

Fig. 4.5. Energy nomenclature.

$$E = z + y + \frac{V^2}{2g} \quad . \tag{4.3}$$

The power at any given cross section of the conduit is found by multiplying the energy at its section by the weight rate of flow past the section. The power equation then can be written as

$$P = \gamma Q E \tag{4.4}$$

or

$$P = \gamma Q\left(z + y + \frac{V^2}{2g}\right) \quad , \tag{4.5}$$

in which P is the power in foot-pounds per second, Q is the volume rate of flow in cubic feet per second, and γ is the specific weight of water in pounds per cubic foot.

Power computations. For each set of flow conditions, power was evaluated at three sections. These sections were: the main conduit section upstream from the junction box, the main conduit section downstream from the junction box, and a lateral section immediately before the lateral entry into the junction box.

Power in the main conduit. The power entering the junction box from the main conduit was calculated by first computing the energy E at each of the stations measured. The energy grade line was then computed by taking a least-squares regression line through five of the energies computed. The energy grade line was linearly projected to the center of the junction box. The power from the main flow into the junction was computed by multiplying the projected energy at the center of the junction box by the main flow in cubic feet per second and by the specific weight of the water.

The computation of power downstream from the junction was made in a similar manner to computations made for the upstream power.

Power contributed to the junction box by the lateral inflow was similarly computed. In this case it was necessary to consider both the difference in elevation between the lateral conduit invert and the main conduit invert, and the depth of flow in the lateral conduit or the piezometric head of the lateral conduit at full flow.

In the case of the lateral flow with the lower inlet, the inlet can be submerged or flowing partially full. As all experiments were carried out with non-submerged lateral inlets, the power of lateral inflow was determined by the conditions of full lateral pipe flow as existed a short distance upstream of the inlet. This power is then

$$P = \gamma Q_\ell \left(\frac{Q_\ell^2}{2gA_\ell^2} + D_\ell + z\right) \quad , \tag{4.9}$$

in which A_ℓ is the area of the lateral inlet conduit and D_ℓ is the diameter of the lateral conduit. The term z is zero since the zero datum was taken at the invert in the center of the junction box.

Using the lower inlet of the lateral inflow into the junction box and with submerged flow the power input was evaluated by

$$P = \gamma Q_\ell \left(\frac{Q_\ell^2}{2gA_\ell^2} + \bar{y} + z\right) \quad . \tag{4.10}$$

The term z is again zero. The depth of water in the junction box is denoted as $\bar{y}$ and was determined by averaging the depth readings immediately upstream and downstream of the junction box.

When using the upper inlet of lateral inflow into the junction box, with free-surface flow into the main conduit, the power input was evaluated by the relation

$$P = \gamma Q_\ell \left(\frac{V_c^2}{2g} + y_c + z_u \right) \quad , \qquad (4.11)$$

in which y_c is the critical depth for the given flow conditions, V_c is the critical velocity, and z_u is the vertical distance from the datum to the invert of the upper inlet. Critical depth and critical velocity were evaluated by the expression

$$\frac{gA^3}{Q^2 B} = 1 \quad , \qquad (4.12)$$

in which A is the cross sectional area, B is the top width, Q is the rate of flow, and g is the gravity acceleration.

Analysis and results. In order to relate the energy losses for various flow conditions, the data were made dimensionless by expressing the power losses as ratios of power inputs in the form

$$P_r = \frac{\gamma Q_m E_m + \gamma Q_\ell E_\ell - \gamma Q_d E_d}{\gamma Q_m E_m + \gamma Q_\ell E_\ell} \quad , \qquad (4.13)$$

in which P_r is the ratio of power lost in the junction box to the power entering the junction, the subscript m referring to the upstream conditions or the inflow to the junction box from the main conduit, the subscript ℓ referring to the lateral inflow conditions, and the subscript d referring to the downstream conditions or the outflow from the junction box. The above Eq. 4.13 is thus an expression of efficiency of the given geometry and flow conditions at the junction boxes.

It was assumed that the power loss ratio P_r could be expressed as a function of the relative discharge of the lateral to the main conduit flow when using the upper inlet ($Q_r = Q_\ell / Q_m$). The validity of this assumption is demonstrated in Fig. 4.6. The functional relation between the power loss ratio and the discharge ratio was developed. The fitted equation to the points in Fig. 4.6 is

$$(P_r - 0.77)(Q_r + 0.55) = -0.482 \quad . \qquad (4.14)$$

Equation 4.14 was used for all subsequent numerical computations for losses produced at the junction box when lateral inflow was introduced at the upper inlet. Equation 4.14 is applicable for values of Q_r between 0.1 and 6.0. Within this range the standard error in estimating P_r is 0.0218. For Q_r values less than 0.1, the power loss ratio is less than 0.03. When there is no lateral inflow and the depth of flow in the main conduit is less than one-half full, the power loss through the junction box is the same as for the straight, undisturbed conduit.

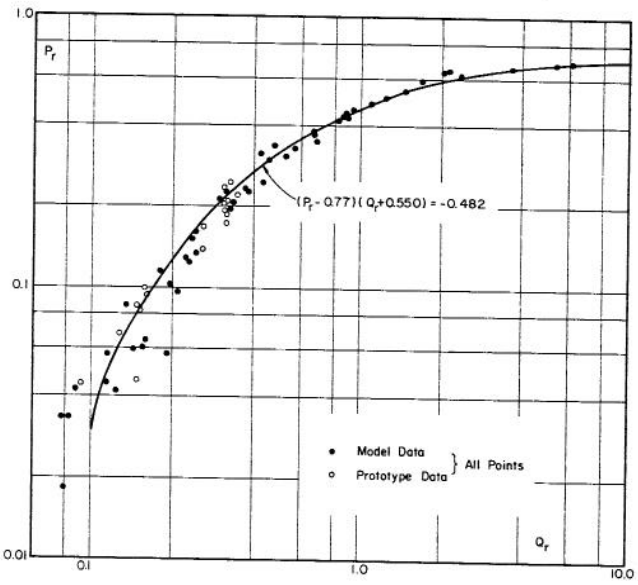

Fig. 4.6. The P_r versus Q_r relationship for the upper inlet of laterals.

Power losses for the lower inlet of lateral inflow at the junction box were analyzed in terms of the ratio of lateral inflow discharge to the main conduit discharge, and the ratio of the upstream depth to the conduit diameter. A plot of the data points is presented in Fig. 4.7. A functional relation of these data points was developed and the resultant power loss ratio is

$$P_r = \frac{-2.78 + 1.71\ D_r}{Q_r + 3.122 - 0.167\ D_r} + 0.77. \qquad (4.15)$$

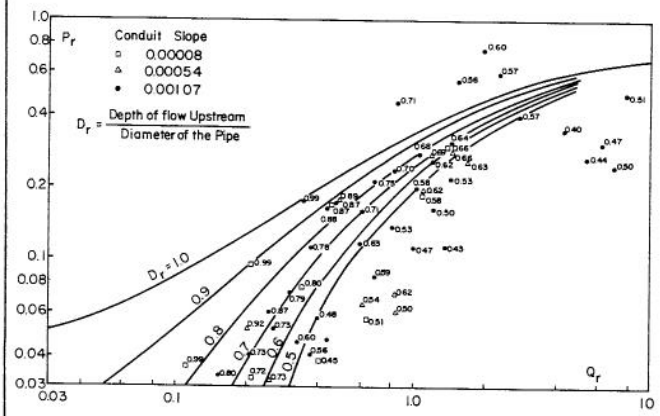

Fig. 4.7. The P_r versus Q_r for various D_r relationship for the lower inlet of laterals.

The standard error in estimating P_r for given values of Q_r is 0.082. Disregarding the values of D_r of less than 0.5, the standard error in estimating P_r for given values of Q_r is 0.067. The estimated values of P_r apply for the range of Q_r from approximate 0.15 to 0.8. The depth ratio D_r range is from 0.40 to 0.99 of the main conduit diameter as represented by each data point in Fig. 4.7.

The computer programs for evaluating the effects of lateral inflow used an improved functional relationship over that expressed by Eq. 4.15. The least squares fitted equation is

$$z = a_1x + a_2y + a_3x^2 + a_4y^2 + a_5xy + a_6 \qquad (4.16)$$

in which $z = D_r$, $x = \log_{10} Q_r$, $y = \log_{10} P_r$, and $a_1 = -1.129$, $a_2 = 1.045$, $a_3 = 0.662$, $a_4 = 0.376$, $a_5 = -0.753$, and $a_6 = 1.045$.

4.5 Effect of the Junction Boxes on Downstream Conduit Flow Resistance

For each of the run conditions used to develop the power loss ratios at the junction box, data were collected to evaluate the hydraulic boundary resistance downstream of the junction box. These values were consistently higher than the values of hydraulic resistance computed upstream of the junction box.

An explanation of this observation involves two factors. The first factor is the increased turbulence introduced into the main conduit flow by the lateral inflow and the junction-box geometry. All the lateral inflows studied intersected the main conduit at 90° to the main conduit centerline. The intersecting flow had to traverse a right angle turn as well as undergo a change in the particle velocities. This combined motion produces standing surface waves and an internal rotational motion superimposed on the main conduit flow. This higher velocity near the solid boundary increases boundary shear and hence the boundary resistance. The effect persists downstream until the normal depth is approached which in this experiment was about 50 pipe diameters.

The second factor is the experimental difficulties in measuring the water surface due to the transverse waves and longitudinal surges generated by the instabilities in the junction box. In spite of the measurement difficulties, the analysis of data show consistencies in the means of junction hydraulic parameters, but with relatively wide scattering of points about the fitted curves.

The observed hydraulic friction factors of the Darcy-Weisbach equation are presented in Fig. 4.8 for the downstream main conduit section of upper and lower inlet postions, as well as for the upstream main conduit section. Within the upstream reach, with no flow disturbance produced by lateral inflow, the friction factor ranges approximately between 0.010 and 0.020. Downstream of the junction box, with lateral inflow from the upper inlet, the friction factor ranges between 0.020 and 0.030 with a tendency toward the lower end of the range. Downstream of the junction box, with lateral inflow from the lower inlet, the friction factors range approximately between 0.010 and 0.030 with a tendency to cluster around a value of 0.020.

From the preceding discussion, it is concluded that the energy losses resulting from lateral inflow into a junction box consist of two components: the immediate energy losses during the change in direction of the lateral flow and the gradual decay of turbulence in the channel downstream of the junction. The former has been evaluated and related to the significant parameters of geometry and flows. The latter has not been evaluated in a manner which would permit application to general use.

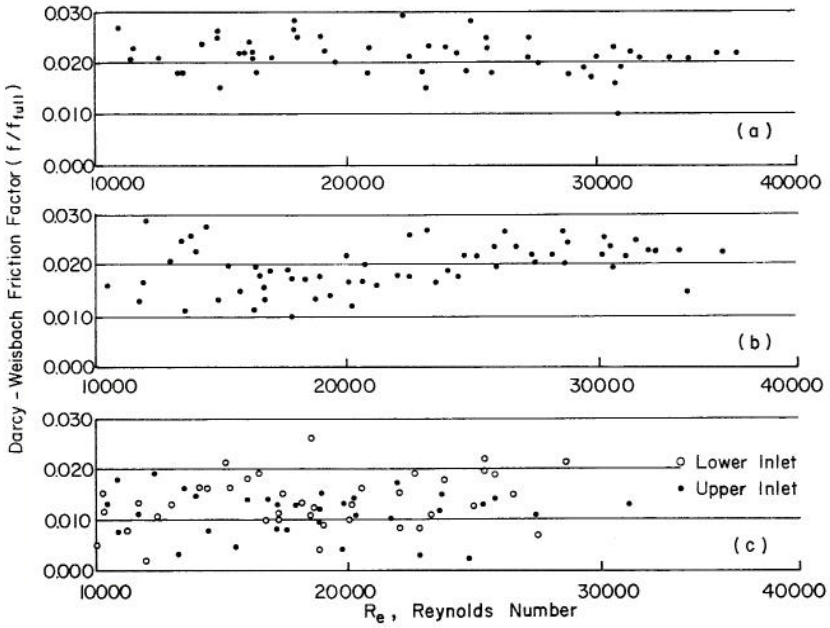

Fig. 4.8. The relation of friction factor f versus Reynolds number R_e: (a) downstream, upper inlet, (b) downstream, lower inlet and (c) upstream, upper and lower inlets.

Chapter 5

VELOCITY DISTRIBUTION COEFFICIENTS

5.1 Definition of Velocity Distribution Coefficients

Equations which define the velocity distribution coefficients are based on momentum and energy considerations, respectively. This may be demonstrated as follows. Momentum due to a motion of an incompressible fluid may be expressed as

$$M = \int_A \rho v \, |v| \, dA \, , \tag{5.1}$$

in which $\rho|v|dA$ describes the mass of water passing through the area dA of a cross section in a unit of time. The integrals in the following text are over the cross sectional area A and the limit A will be deleted in these expressions.

One-dimensional considerations give

$$M = \rho \int v^2 dA \, . \tag{5.2}$$

An approximation to this evaluation of one-dimensional momentum flux is to represent it in terms of the mean velocity V as,

$$M = \beta\rho \, V^2 A \, . \tag{5.3}$$

The coefficient β is then defined as

$$\beta = \frac{\int v^2 dA}{V^2 A} \, . \tag{5.4}$$

The constant in the equation of kinetic energy per unit weight correspondingly develops into the form

$$\alpha = \frac{\int v^3 dA}{V^3 A} \, . \tag{5.5}$$

Thus, the general theoretical form of a velocity distribution coefficient of n-th order is represented for the velocity v at a point raised to the power n by

$$\phi = \frac{\int v^n dA}{V^n A} \, , \tag{5.6}$$

in which equation n takes on only integer values. For n equal to one, the coefficient ϕ is unity, which by definition is the mean velocity. Values of $n = 2$ and $n = 3$ in Eq. 5.6 give the momentum (β) and energy (α) velocity distribution coefficients, respectively.

Equation 5.6 permits the evaluation of the effect of velocity distributions in a cross section on α and β, and the computation of interrelation between α and β.

5.2 Approximate Relation Between α and β Coefficients

Consider the time-average velocity at a point as

$$v = (1+k) \, V \, , \tag{5.7}$$

in which V is the mean velocity across a cross section of point time-average velocities and k is plus or minus depending on the position of a point. Since the mean velocity V is defined as

$$V = \frac{1}{A} \int v dA = \frac{1}{A} \int (1+k) V dA = V + \frac{V}{A} \int k dA,$$

the integral kdA over the area A must be zero.

When β and α are expressed in terms of k, then

$$\beta = \frac{\int V^2 (1+k)^2 dA}{V^2 A} = 1 + \frac{1}{A} \int k^2 dA \, , \tag{5.8}$$

and

$$\alpha = \frac{\int V^3 (1+k)^3 dA}{V^3 A} = 1 + \frac{3}{4} \int k dA + \frac{3}{A} \int k^2 dA + \frac{1}{A} \int k^3 dA \, .$$

Because the integral of kdA is zero,

$$\alpha = 1 + \frac{3}{A} \int k^2 dA + \frac{1}{A} \int k^3 dA \, . \tag{5.9}$$

From Eqs. 5.8 and 5.9 the following conclusions may be derived:

(a) The larger the deviation of the point velocities from the mean, the larger are the values of the velocity distribution coefficients, α and β.

(b) For the case when maximum velocity is less than twice the mean velocity, the absolute value of k will be less than one and in that case $0 < \left|\int k^3 dA\right| < \int k^2 dA$.

(c) As the value of k approaches zero, the k^3 - term becomes less significant compared with the k^2 - term, and hence, as an approximation,

$$\frac{\alpha-1}{\beta-1} \simeq 3 \, , \tag{5.10}$$

or $\alpha \simeq 3\beta - 2$.

The values of α and β determined experimentally in this study tend to confirm this approximate relation.

5.3 Evaluation of Velocity Distribution Coefficients

Equation 5.6 suggests several methods of evaluating the velocity distribution coefficients, ϕ. One method is the analytical integration of a given time-average velocity distribution function over the cross section, the other two being the graphic and numerical methods of integration using point time-average velocities observed in a specific flow by a replacement of integrals by summations.

Analytical Integration Method. The analytical integration of Eq. 5.6 depends on a knowledge of the explicit function of velocity as related to position. Such equations for fully developed turbulent flow are available only for certain limiting cases of boundary configuration.

For the case of an infinitely-wide open channel with two-dimensional flow the following equation has been determined experimentally for velocity distributions outside the boundary layer [4]:

$$\frac{(v-V)}{V\sqrt{f}} = 2 \log_{10} \frac{y}{y_o} + 0.88 \quad , \tag{5.11}$$

in which v is the point velocity at position y, V is the mean velocity for depth y_o and f is the friction factor in the Darcy-Weisbach equation. Substituting the value of v from Eq. 5.11 into Eq. 5.6, and integrating in the limits from zero to y_o, ϕ - coefficients for values of $n = 2$ and $n = 3$ are, respectively,

$$\beta = \phi_2 = 1.0 + 0.755\ f + 0.023\ \sqrt{f} + \delta_1(f) \tag{5.12}$$

and

$$\alpha = \phi_3 = 1.0 + 2.263\ f + 0.035\sqrt{f} - 1.284\ f\sqrt{f} + \delta_2(f), \tag{5.13}$$

in which $\delta_1(f)$ and $\delta_2(f)$ represent the negligible effects of boundary layers. In this case, the ϕ - functions are the result of integrating Eq. 5.11 from the limit of the boundary layer rather than from the solid boundary. In each case, however, the velocity distribution functions of the boundary layer have a negligible effect on the respective velocity distribution coefficients. The plots of these equations are shown in Fig. 5.1 as the computed α and β values of partly flowing conduits. Within this range of friction factors the theoretical dependencies of α and β coefficients on f are approximately linear for values of f greater than 0.004.

It is interesting to note that the ratio of $(\alpha-1)/(\beta-1)$ lies approximately between 2.5 and 2.6 as shown in Fig. 5.2. The fact that the ratio of 3.0 of Eq. 5.10 does not agree with the range 2.5 - 2.6 as developed for the logarithmic velocity distribution in an infinitely-wide channel indicates that, for that case at least, the integral of the k^3 - term must be significant as well as negative.

For the case of a full flow in a circular conduit, the following equation has been determined experimentally to be the velocity distribution function [4]:

$$\frac{v-V}{V\sqrt{f}} = 2 \log_{10} \left(\frac{y}{r_o}\right) + 1.32 \quad , \tag{5.14}$$

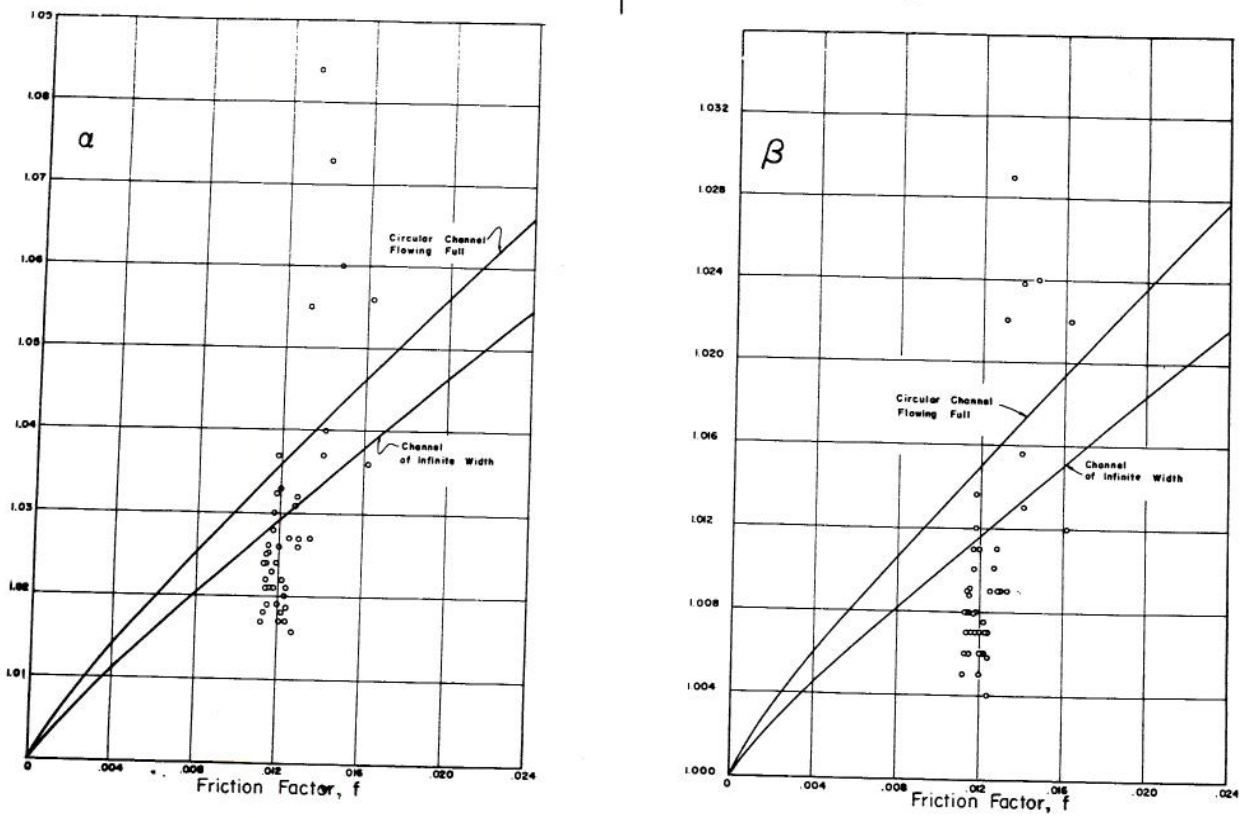

Fig. 5.1. Theoretical relation and CSU experimental points of velocity distribution coefficients versus friction factor f.

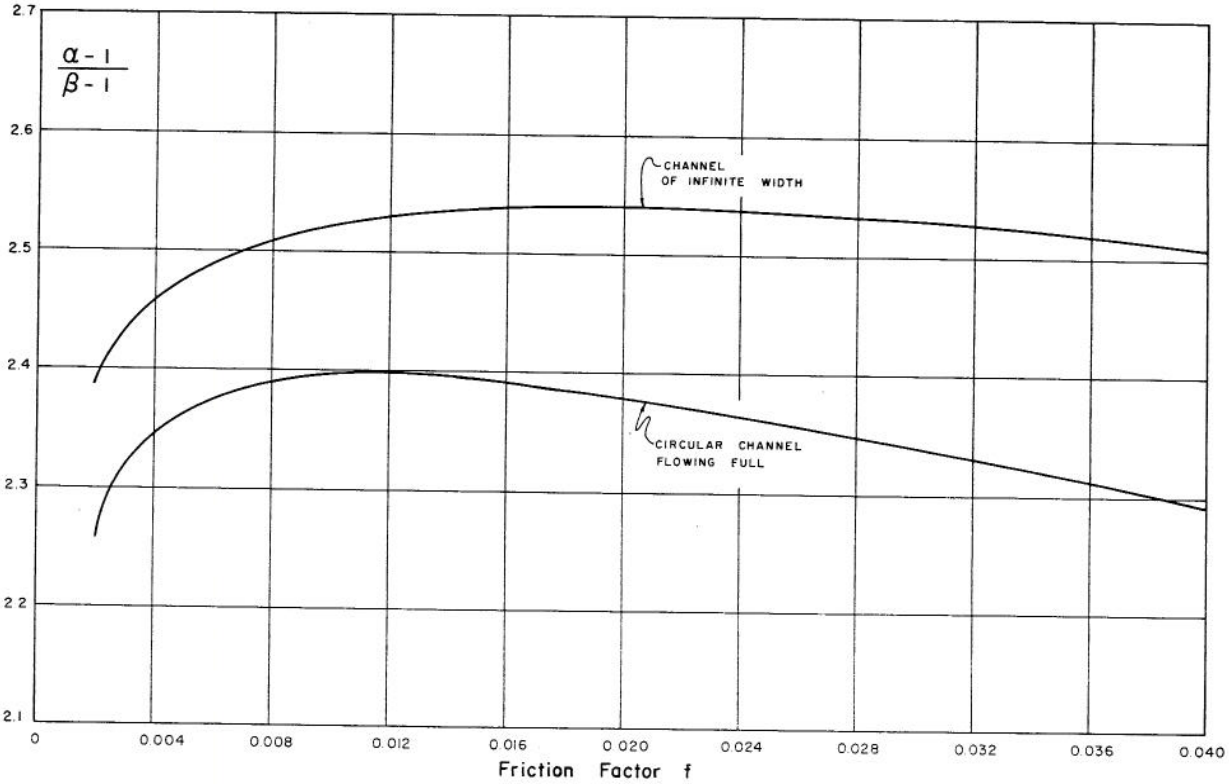

Fig. 5.2. Relation of α and β versus friction factor f.

in which the variables are defined as before, and r_o is the radius of the conduit. Substituting the value of v from Eq. 5.14 into Eq. 5.6 and solving for ϕ within the limits of boundary thickness (δ) and r_o one obtains respectively

$$\beta = \phi_2 = 1 + 0.034\sqrt{f} + 0.941\, f \qquad (5.15)$$

and

$$\alpha = \phi_3 = 1 + 0.051\sqrt{f} + 2.828\, f - 2.685\, f\sqrt{f} \quad . \qquad (5.16)$$

The values of α and β from Eqs. 5.15 and 5.16 are also plotted in Fig. 5.1. These curves approach straight lines for a large range of f-values. Similarly, as in the case of an infinitely-wide open channel, α and β coefficients depend only on the friction factor f. In this case, the ratio $(\alpha-1)/(\beta-1)$ also lies approximately between 2.3 and 2.4, as shown in Fig. 5.2.

Because the velocity distributions are often non symmetrical around the mean velocity, the integral $\int k^3 dA$ may be negative if the absolute values of the negative k are much greater than the absolute values of the positive k. This is the case in the velocity distributions of both the infinitely-wide open channel and the full pipe flow as given by Eqs. 5.11 and 5.14 while using a lower limit of zero. Therefore, $(\alpha-1)/(\beta-1)$ being smaller than 3.0 is expected.

The comparison of curves of Eqs. 5.15 and 5.16 with the corresponding curves for β and α of Eqs. 5.12 and 5.13 in Fig. 5.1 indicates that for channels in which the side walls substantially affect the velocity distributions (or when the height of sides is of the same order of magnitude as the width of the channel bottom) the k - values, on the average, are greater than the k values for infinitely-wide open channels. Hence, the α and β-coefficients are greater for full flows in circular conduits.

Because velocity distributions in partial flows through circular conduits can be considered cases which are between the velocity distributions of an infinitely-wide open channel and a full flowing circular conduit, Eqs. 5.12, 5.13, 5.15 and 5.16 give an indication and a range of the expected velocity distribution coefficients as they change with the friction factor f.

Graphic integration method. The classic method for computing velocity distribution coefficients from observed data is to plot the position of observed velocities along with the velocity at that point. The lines of equal velocity (isovels) are then drawn by interpolating between the known velocities. The area between successive incremental velocities is then determined, for example, by a planimeter. The summation of the individual areas times the mean velocity in the area taken to the appropriate power (2 or 3), provides the numerical integration of the numerator of β and α. A sample of the result is shown in Fig. 5.3.

Numerical integration method. A numerical integration method was developed around the point velocity measurement equipment. Time-average point velocities were measured by Ott current meters. Five meters were mounted on a center-supported rod which was then placed at the conduit centerline. The rod support could rotate to place the meters in any angular position. The meters were spaced along the

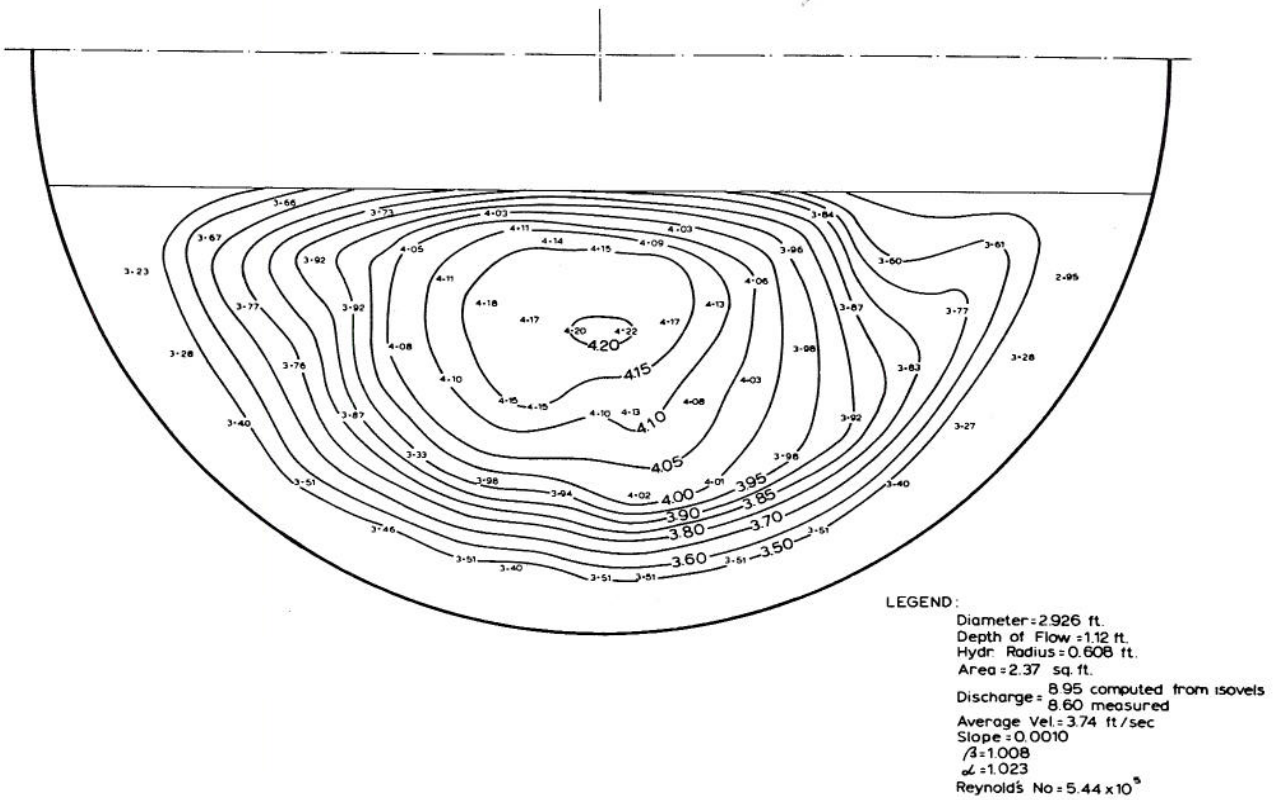

Fig. 5.3. Isovels (equal velocity lines) for partially full conduit flow.

rod to sample equal annular areas and the end meter was placed at the minimum recommended distance from the pipe wall. The support rod of the meters was positioned at angular intervals of 10 degrees and point velocities were observed at five radial positions using as many 10-degree intervals as required to sample the circular segment.

Data processing was based on the observation that velocity distributions along the radial directions and along circumferential arcs of constant radius were smooth and could be approximated by third-degree polynomials.

The computer procedure was as follows:

1. A third-degree polynomial was fitted to the observed velocities at a fixed radius, of the form

$$v_r = a_r + b_r\theta + c_r\theta^2 + d_r\theta^3 \quad . \tag{5.17}$$

2. For a given angular position, a third-degree polynomial was fitted to the computed velocities along the radial direction, of the form

$$v_\theta = a_\theta + b_\theta r + c_\theta r^2 + d_\theta r^3 \quad . \tag{5.18}$$

3. For the velocity expression at a given angular position, the integrals of $v_\theta dA$, $v_\theta{}^2 dA$ and $v_\theta{}^3 dA$ are obtained, in which dA was the area represented by a 10-degree sector to the free-water surface.

4. The results of Step 3 divided by the appropriate relation of the mean velocity and the total area resulted in α and β coefficients.

The root-mean-square difference between the observed velocities and the computed velocities (based on the polynomial fitting procedure) was computed for each case of measurement of velocity distributions of partly full conduits. The calibration equations for each current meter and propeller were included in the computer program so that the velocity was computed from the given data before polynomial fitting was begun.

5.4 Results of Experimental Investigations

Several comparisons of test conditions and observational procedures were made to identify their effects on the computed velocity distributions. These considerations were reproducibility of results, effects of depth, location along the conduit, number of point velocities, and length of time for observing the mean velocity. The results of these evaluations are presented in Table 5.1. This table gives data in the following order: run identification (RUN NO.), discharge in cubic feet per second as measured by the inflow orifice (DISCH), depth of flow in feet at the measurement cross section (DEPTH), cross sectional area in square feet (AREA), mean-velocity in feet per second based on the measured discharge (VEL), number of point velocity observations (N), average number of point observations per square foot (N/A), ratio of the mean velocity based on the measured discharge compared to the mean velocity obtained by integrating the observed velocities (GAMMA), momentum velocity distribution coefficient (BETA), energy velocity distribution coefficient (ALPHA), the root-mean square difference between the observed velocities

TABLE 5.1. Reproducibility and effects of various factors on velocity distribution coefficients

RUN NO	DISCH	DEPTH	AREA	VEL	N	N/A	GAMMA	BETA	ALPHA	STDDEV	TIME
Reproducibility											
X7MH2A	26.340	2.210	5.449	4.834	146	26.79	1.006	1.006	1.018	0.051	
X7MH2B	26.340	2.139	5.268	5.000	144	27.34	1.008	1.005	1.017	0.081	
X10M2A	16.130	1.612	3.797	4.248	91	23.96	1.025	1.011	1.030	0.041	
X10M2B	16.130	1.597	3.754	4.297	91	24.24	1.028	1.011	1.029	0.035	
Effect of Depth											
X12M2A	8.260	1.064	2.209	3.739	33	14.94	0.920	1.066	1.123	0.037	
X6MH2A	13.450	1.442	3.301	4.075	70	21.21	1.037	1.005	1.019	0.037	
X10M2A	16.130	1.612	3.797	4.248	91	23.96	1.025	1.011	1.030	0.041	
X9MH2C	20.520	1.888	4.588	4.472	122	26.59	1.025	1.006	1.019	0.047	
X8MH2X	24.240	2.079	5.110	4.744	140	27.40	1.002	1.009	1.027	0.042	
X7MH2A	26.340	2.210	5.449	4.834	146	26.79	1.006	1.006	1.018	0.051	
Effect of Position in Direction of Flow											
X8MH1A	23.930	2.110	5.192	4.609	148	28.51	1.011	1.009	1.025	0.058	
X8MH2X	24.240	2.079	5.110	4.744	140	27.40	1.002	1.009	1.027	0.042	
X8MH3A	24.240	2.063	5.067	4.783	144	28.42	1.007	1.007	1.021	0.048	
X9MH1C	20.520	1.909	4.647	4.416	123	26.47	1.014	1.006	1.019	0.094	
X9MH2C	20.520	1.888	4.588	4.472	122	26.59	1.025	1.006	1.019	0.047	
X9MH3C	20.520	1.880	4.566	4.494	121	26.50	1.024	1.008	1.024	0.046	
X10M1A	16.130	1.617	3.812	4.231	94	24.66	1.006	1.010	1.028	0.044	
X10M2A	16.130	1.612	3.797	4.248	91	23.96	1.025	1.011	1.030	0.041	
X10M3A	16.130	1.611	3.795	4.251	91	23.98	1.017	1.011	1.030	0.045	
Effect of Number of Point Velocities											
X8MH2X	24.240	2.079	5.110	4.744	140	27.40	0.999	1.010	1.028	0.029	
X8MH2Y	24.240	2.094	5.150	4.707	73	14.18	1.012	1.008	1.022	0.049	
Effect of Length of Time of Observations											
X6MH2A	13.450	1.442	3.301	4.075	70	21.21	1.037	1.005	1.019	0.037	30
X6MH2A	13.450	1.442	3.301	4.075	70	21.21	1.034	1.005	1.020	0.028	60
X6MH2A	13.450	1.442	3.301	4.075	70	21.21	1.032	1.005	1.019	0.021	90
X6MH2A	13.450	1.442	3.301	4.075	70	21.21	1.031	1.005	1.020	0.018	120
X6MH2A	13.450	1.442	3.301	4.075	70	21.21	1.031	1.005	1.019	0.018	150
X6MH2A	13.450	1.442	3.301	4.075	70	21.21	1.032	1.006	1.020	0.101	180
X8MH2X	24.240	2.079	5.110	4.744	140	27.40	1.002	1.009	1.027	0.042	30
X8MH2X	24.240	2.079	5.110	4.744	140	27.40	0.999	1.010	1.028	0.029	60
X8MH2X	24.240	2.079	5.110	4.744	140	27.40	0.999	1.009	1.027	0.029	90
X8MH2X	24.240	2.079	5.110	4.744	140	27.40	0.999	1.009	1.027	0.030	120
X8MH2X	24.240	2.079	5.110	4.744	140	27.40	0.998	1.009	1.027	0.030	150
X8MH2X	24.240	2.079	5.110	4.744	139	27.20	0.998	1.009	1.027	0.030	180
X8MH2Y	24.240	2.094	5.150	4.707	73	14.18	1.012	1.008	1.022	0.049	30
X8MH2Y	24.240	2.094	5.150	4.707	74	14.37	1.013	1.008	1.022	0.039	60
X8MH2Y	24.240	2.094	5.150	4.707	73	14.18	1.011	1.008	1.023	0.032	90
X8MH2Y	24.240	2.094	5.150	4.707	73	14.18	1.010	1.008	1.024	0.029	120
X8MH2Y	24.240	2.094	5.150	4.707	73	14.18	1.010	1.008	1.024	0.030	150
X8MH2Y	24.240	2.094	5.150	4.707	73	14.18	1.010	1.008	1.024	0.026	180

and the velocities in feet per second computed from the polynomial fits (STDDEV), and the observed time interval in seconds used to compute the mean velocity.

These results were not intended to be conclusive. They do provide, however, a measure of effect and reliability of the overall results.

The general observations on these data are:

(a) The root-mean-square (STDDEV), as a percent of the mean velocity, is of the order of 1 percent.

(b) The computed mean velocity is larger than the measured mean velocity by less than 3 percent in most cases.

(c) The relation between α and β coefficients conforms approximately with Eq. 5.10.

(d) The variation of the velocity distribution coefficients within any one of five effect categories is insufficient to detect a clear effect over the entire sample size. In other words, the experimental and computational errors overshadow the effect of varying the experimental conditions.

Based on the preliminary results of Table 5.1, an extended series of observations were made to relate the velocity distribution coefficients to the depth and the mean velocity. The observations were made at the midpoint of the 822 foot conduit. Each point velocity was averaged over a 60-second period. The results of these observations are presented in Table 5.2.

TABlE 5.2. Velocity distribution coefficients in the conduit of 2.926 feet in diameter.

Designation	Slope	Depth ft	Hydraulic Radius R, ft	Discharge Q cfs	Mean Velocity fps	$Re = \frac{VR}{\nu}$ x 10^5	α	β	Friction Factor f
S1-4	0.000032	2.926	0.732	5.610	0.834	0.4	1.036	1.012	0.0162
S1-7		1.547	0.757	11.980	3.320	1.653	1.017	1.004	0.0124
S1-8		1.779	0.818	16.040	3.748	2.017	1.019	1.006	0.0120
S1-9		1.984	0.857	19.620	4.042	2.278	1.021	1.007	0.0118
S2-2	0.000132	1.749	0.811	10.080	2.404	1.283	1.026	1.009	0.0129
S2-3		2.064	0.869	15.340	3.026	1.736	1.020	1.007	0.0123
S2-4		2.371	0.890	18.940	3.245	1.900	1.017	1.006	0.0121
S2-5		2.630	0.873	19.570	3.073	1.765	1.018	1.006	0.0122
S2-6		1.152	0.620	4.710	1.915	0.781	1.040	1.013	0.0141
S2-9		0.903	0.512	3.260	1.848	0.622	1.060	1.024	0.0147
S2-10		1.785	0.819	16.640	3.873	2.087	1.024	1.008	0.0119
S2-10		1.936	0.849	16.640	3.524	1.968	1.021	1.007	0.0120
S3-1	0.000520	2.644	0.870	18.350	2.870	1.643	1.021	1.007	0.0124
S3-2		2.309	0.889	12.270	2.156	1.261	1.027	1.009	0.0130
S3-3		2.079	0.870	14.100	2.756	1.577	1.027	1.009	0.0125
S3-4		1.740	0.809	10.410	2.498	1.330	1.032	1.011	0.0128
S3-5		1.497	0.742	7.960	2.299	1.122	1.055	1.022	0.0132
S3-6		1.154	0.620	6.210	2.519	1.028	1.084	1.029	0.0134
S3-7		0.871	0.497	2.040	1.215	0.397	1.056	1.022	0.0163
S3-10		1.771	0.816	15.970	3.752	2.014	1.033	1.011	0.0120
D2A	0.001022	0.810	0.468	4.000	2.637	0.812	1.073	1.024	0.0140
D2B		0.817	0.471	4.000	2.605	0.807	1.037	1.016	0.0140
D3C		1.964	0.854	8.220	1.713	0.962	1.027	1.009	0.0135
D7A		1.989	0.858	23.380	4.803	2.711	1.024	1.008	0.0114
D7C		2.357	0.890	23.380	4.028	2.358	1.021	1.007	0.0116
D8B		2.166	0.880	25.620	4.800	2.779	1.024	1.008	0.0113
X6MH2A	0.001001	1.442	0.725	13.450	4.075	1.944	1.019	1.005	0.0120
X7MH2A		2.210	0.884	26.340	4.835	2.812	1.018	1.006	0.0113
X7MH2B		2.139	0.878	26.340	5.000	2.888	1.017	1.005	0.0112
X8MH1A		2.110	0.874	23.930	4.609	2.650	1.025	1.009	0.0114
X8MH2X		2.079	0.871	24.240	4.744	2.718	1.027	1.009	0.0114
X8MH24		2.094	0.873	24.240	4.707	2.703	1.022	1.008	0.0114
X8MH3A		2.063	0.869	24.240	4.783	2.734	1.021	1.007	0.0114
X9MH1C		1.909	0.844	20.520	4.416	2.452	1.019	1.006	0.0115
X9MH2C		1.888	0.841	20.520	4.472	2.474	1.019	1.006	0.0115
X9MH3C		1.880	0.839	20.520	4.494	2.481	1.024	1.008	0.0115
X10M1A		1.617	0.777	16.130	4.231	2.163	1.028	1.010	0.0117
X10M2A		1.612	0.776	16.130	4.248	2.169	1.030	1.011	0.0117
X10M3A		1.611	0.775	16.130	4.251	2.167	1.030	1.011	0.0117
X10M2B		1.597	0.772	16.130	4.297	2.182	1.030	1.011	0.0117
X12M1A		1.090	0.843	8.260	3.618	2.006	1.035	1.007	
X12M2A		1.064	0.583	8.260	3.739	1.434	1.123	1.066	
X12M2B		1.372	0.701	8.260	2.668	1.230	1.095	1.040	
X12M2C		1.066	0.583	8.300	3.747	1.437	1.024	(1)	
D3A	0.001022	1.057	0.580	8.220	3.754	1.432	1.031	1.010	0.0127
D3B		1.078	0.589	8.220	3.655	1.416	1.016	(1)	0.0127
D4C		1.903	0.843	12.920	2.790	1.666	1.019	1.006	0.0124
D5A		1.605	0.774	16.000	4.236	2.157	1.032	1.012	0.0118
D5B		1.601	0.772	16.000	4.249	2.159	1.037	1.014	0.0118
D5C		2.187	0.882	16.000	2.968	1.718	1.022	1.008	0.0122
D6A		1.855	0.834	20.510	4.562	2.503	1.025	1.009	0.0115
D6B		1.868	0.837	20.510	4.526	2.492	1.026	1.009	0.0115
D6C		2.198	0.883	20.510	3.785	2.199	1.023	1.008	0.0117

(1) Computed value less than the minimum value of one.

5.5 Discussion of Experimental Results

It was expected that the velocity distribution coefficients would differ with changes in those parameters which determine the velocity profiles. The parameters which primarily effect the velocity profile are the geometry of the cross section, the properties of the fluid, the condition of the boundary surface (roughness), and the mean velocity. All of these variables are encompassed in the Reynolds number (VR/ν) and the Darcy-Weisbach friction factor (f).

Because the Darcy-Weisbach friction factor is related to the Reynolds number, one would expect to be able to correlate α and β-coefficients to the friction factor f. The experimentally observed values of α and β in this study are plotted in Fig. 5.1. Since the range of the Darcy-Weisbach friction factor is small for the series of data in this study, and because the Reynolds number fluctuates within a limited range, the spread of computed α and β coefficients is apparently due to other causes.

Figure 5.4 displays the relation of α and β with the Reynolds number. These results indicate an increase of the velocity distribution coefficients with a decrease of Reynolds number. The general trends may be represented by two curves. The apparent scatter of points around these curves may be assigned to observational and computational errors.

The following parameters of the computed velocity distribution coefficients remained essentially constant: the circular form of the section, the fluid properties (water at approximately 45°F), and approximately the friction factor because the Reynolds number varied over a narrow range. It would follow, therefore, that the variation in α and β could be represented as a function of depth and mean velocity or slope as a first approximation. Because the effect of depth and mean velocity are included, through their product, into the Reynolds number (assuming an approximate proportionality of depth and hydraulic radius), the main relation should be between the velocity distribution coefficients and the Reynolds number.

The effect of depth on the velocity distribution coefficients is presented in Table 5.3 and Fig. 5.5. The values in Table 5.3 are grouped in ascending order of the depth-diameter ratio (y/D). The corresponding mean velocities (V) which are also listed do not arrange themselves in any discernable manner. This is probably because the mean velocity increases with the depth for a given slope and roughness, and the depth has already accounted for the effects of the mean velocity. Figure 5.5 indicates slightly increasing values of both β and α as depth decreases. This is expected because deviation from the mean velocity becomes greater and the friction factor becomes effectively larger as the depth decreases.

At a depth of half the conduit diameter β - coefficient has a value of approximately 1.01 and α - coefficient of approximately 1.03. At greater depths β reduces to approximately 1.007 and α reduces to approximately 1.022. For depths less than half the conduit diameter, both coefficients tend to increase. Data was not available for depths less than one-fourth of a diameter.

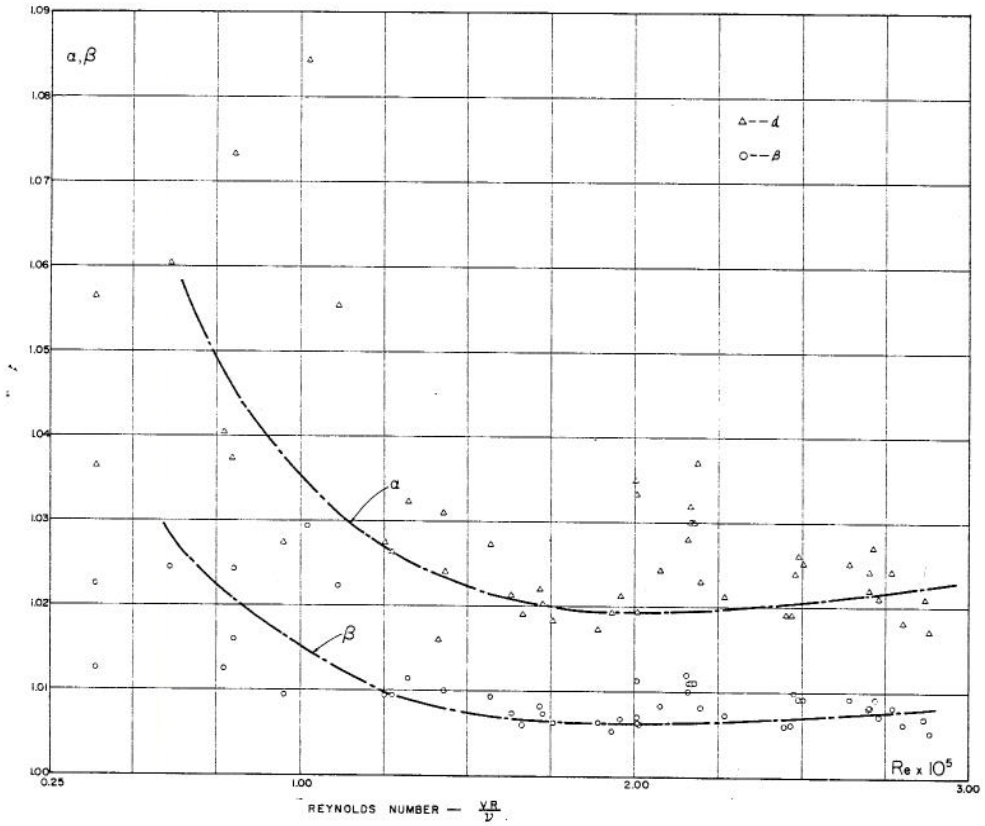

Fig. 5.4. Velocity distribution coefficients versus Reynolds number.

TABLE 5.3. Velocity distribution coefficients as a function of depth.

Range of Depth ft.	Run No.	Depth-Diameter Ratio	Depth y,ft	Velocity V,fps	α	β
0-1.0	D2A	0.276	0.810	2.637	1.073	1.024
	D2B	0.279	0.817	2.605	1.037	1.016
	S3-7	0.297	0.871	1.215	1.056	1.022
	S2-9	0.310	0.903	1.848	1.060	1.024
1.0-1.5	D3A	0.360	1.057	3.754	1.031	1.010
	X12M2A	0.363	1.064	3.739	1.123	1.066
	X12M2C	0.366	1.066	3.747	1.024	(1)
	X12M1A	0.373	1.090	3.618	1.035	1.007
	D3B	0.368	1.078	3.655	1.016	(1)
	S2-6	0.393	1.152	1.915	1.040	1.013
	S3-6	0.394	1.154	2.519	1.084	1.029
	X12M2B	0.468	1.372	2.668	1.095	1.040
	X6MH2A	0.492	1.442	4.075	1.019	1.005
	S3-5	0.510	1.497	2.299	1.055	1.022
1.5-1.8	S1-7	0.528	1.547	3.320	1.017	1.004
	X10M2B	0.545	1.597	4.297	1.030	1.011
	D5B	0.546	1.601	4.249	1.037	1.014
	D5A	0.547	1.605	4.236	1.032	1.012
	X10M3A	0.549	1.611	4.251	1.030	1.011
	X10M2A	0.550	1.612	4.248	1.030	1.011
	X10M1A	0.551	1.617	4.231	1.028	1.010
	S3-4	0.593	1.740	2.498	1.032	1.011
	S2-2	0.596	1.749	2.404	1.026	1.009
	S3-10	0.585	1.771	3.752	1.033	1.011
	S1-8	0.604	1.779	3.748	1.019	1.006
	S2-103	0.609	1.785	3.873	1.024	1.008
1.8-2.1	D6A	0.634	1.855	4.562	1.025	1.009
	D6B	0.638	1.868	4.526	1.026	1.009
	X9MH3C	0.642	1.880	4.494	1.024	1.008
	X9MH2C	0.645	1.888	4.472	1.019	1.006
	D4C	0.650	1.903	2.790	1.019	1.006
	X9MH1C	0.652	1.909	4.416	1.019	1.006
	S2-10	0.660	1.936	3.524	1.021	1.007
	D3C	0.670	1.964	1.713	1.027	1.009
	S1-9	0.677	1.984	4.042	1.021	1.007
	D7A	0.678	1.989	4.803	1.024	1.008
	X8MH3A	0.704	2.063	4.783	1.021	1.007
	S2-3	0.704	2.064	3.026	1.020	1.007
	S3-3	0.709	2.079	2.756	1.027	1.009
	X8MH2X	0.709	2.079	4.744	1.027	1.009
	X8MH24	0.714	2.094	4.707	1.022	1.008
2.1-2.5	X8MH1A	0.720	2.110	4.609	1.025	1.009
	X7MH2B	0.729	2.139	5.000	1.017	1.005
	D8B	0.739	2.166	4.800	1.024	1.008
	D5C	0.746	2.187	2.968	1.022	1.008
	D6C	0.750	1.198	3.785	1.023	1.008
	X7MH2A	0.754	2.210	4.835	1.018	1.006
	S3-2	0.787	2.309	2.156	1.027	1.009
	D7C	0.804	2.357	4.028	1.021	1.007
	S2-4	0.809	2.371	3.245	1.017	1.006
2.5-	S2-5	0.897	2.630	3.073	1.018	1.006
	S3-1	0.902	2.644	2.870	1.027	1.009
	S1-4	0.998	2.926	2.210	1.036	1.012

TABLE 5.4. Velocity distribution coefficients as a function of mean velocity.

Run No.	Velocity V,fps	Depth y,ft	α	β
S3-7	1.215	0.871	1.056	1.022
D3-C	1.713	1.964	1.027	1.009
S2-9	1.848	0.903	1.060	1.024
S2-6	1.915	1.152	1.040	1.013
S3-2	2.156	2.309	1.027	1.009
S1-4	2.210	2.926	1.036	1.012
S3-5	2.299	1.497	1.055	1.022
S2-2	2.404	1.749	1.026	1.009
S3-4	2.498	1.740	1.032	1.011
S3-6	2.519	1.154	1.084	1.029
D2B	2.605	0.817	1.037	1.016
D2A	2.637	0.810	1.073	1.024
X12M2B	2.668	1.372	1.095	1.040
S3-3	2.756	2.079	1.027	1.000
D4C	2.790	1.903	1.019	1.006
S3-1	2.870	2.644	1.027	1.009
D5C	2.968	2.187	1.022	1.008
S2-3	3.026	2.064	1.020	1.007
S2-5	3.073	2.630	1.018	1.006
S2-4	3.245	2.371	1.017	1.006
S1-7	3.320	1.547	1.017	1.004
S2-10	3.524	1.936	1.021	1.007
X12M1A	3.618	1.090	1.035	1.007
D3B	3.655	1.078	1.016	(1)
X12M2A	3.739	1.064	1.123	1.066
X12M2C	3.747	1.066	1.024	(1)
S1-8	3.748	1.779	1.019	1.006
S3-10	3.752	1.771	1.033	1.011
D3A	3.754	1.057	1.031	1.010
D6-C	3.785	2.198	1.023	1.008
S2-10	3.873	1.785	1.024	1.008
D7-C	4.028	2.357	1.021	1.007
S1-9	4.042	1.984	1.021	1.007
X6MH2A	4.075	1.442	1.019	1.005
X10M1A	4.237	1.617	1.028	1.010
D5A	4.236	1.605	1.032	1.012
X10M2A	4.248	1.612	1.030	1.011
D5B	4.249	1.601	1.037	1.014
X10M3A	4.251	1.611	1.030	1.011
X10M2B	4.279	1.597	1.030	1.011
X9MH1C	4.416	1.909	1.019	1.006
X9MH2C	4.472	1.888	1.019	1.006
X9MH3C	4.494	1.880	1.024	1.008
D6B	4.526	1.868	1.026	1.009
D6A	4.562	1.855	1.025	1.009
X8MH1A	4.609	2.110	1.025	1.009
X8MH24	4.707	2.094	1.022	1.008
X8MH2X	4.744	2.079	1.027	1.009
X8MH3A	4.783	2.063	1.021	1.007
D8B	4.800	2.166	1.024	1.008
D7A	4.803	1.989	1.024	1.008
X7MH2A	4.835	2.210	1.018	1.006
X7MH2B	5.000	2.139	1.017	1.005

(1) Computed value less than the minimum value of one.

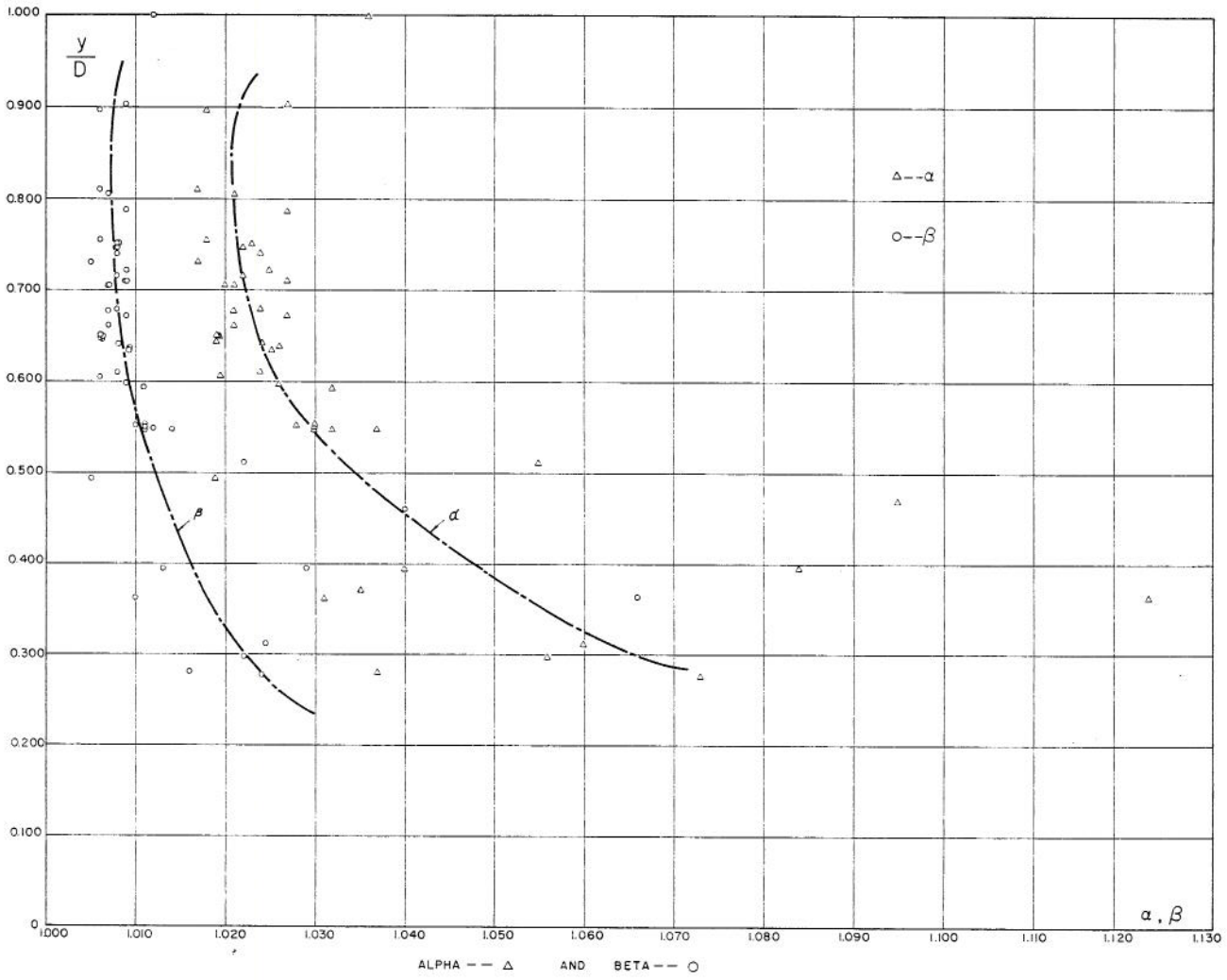

Fig. 5.5. Velocity distribution coefficients versus depth of flow in a circular cross section.

An attempt was made to find a relation between the mean velocity and the velocity distribution coefficients. It may be seen from Table 5.4 that for modest range of depth the variation of mean velocity does not result in a consistent variation in α and β.

Because of the limited range of the Darcy-Weisbach friction factor and the mean velocity, the variation in α and β are identified primarily with the Reynolds number and secondarily with the depth of flow.

5.6 Summary of Results

The results of this study are applicable to hydraulically-smooth circular cross sections flowing partially full and having Reynolds numbers between 0.4×10^5 and 3.00×10^5. In the smaller Reynolds numbers, the observed velocity distribution coefficients are greater but display greater dispersion about a smooth curve. In the larger Reynolds numbers the values trend toward invariance with lesser dispersion. The relation between α and β has been demonstrated both theoretically and experimentally to be expressible as $(\alpha-1)/(\beta-1) = 2.3$ to 3.0. The value of 3.0 is representative of the experimental results. A representative value of α for the experimental conditions is 1.03, and a representative value of β for the experimental conditions is 1.01.

Chapter 6

BOUNDARY CONDITIONS OF EXPERIMENTAL CONDUIT

6.1 Definitions of Boundary Conditions

Adequate knowledge of boundary conditions is necessary for solving the two partial differential equations of gradually varied free-surface unsteady flow. Many physical conditions impose these boundary conditions, which are independent of the solution methods. These boundary conditions must be defined physically and mathematically whenever feasible.

Physical conditions impose boundary conditions on the two quasi-linear hyperbolic partial differential equations of unsteady flow. Five of these conditions follow:

1. The inflow flood hydrograph conditions, described by a specific discharge entering the experimental conduit at each instant of time. The discharge is assumed to be independent of flow conditions in the conduit; hence, the inflows produce no effect on the system. These conditions may be well satisfied in nature, provided no reflected wave tends to alter the discharge-time relation of inflows.

2. The free-outfall conditions at which the depth of flow is considered to be critical. These result in a unique relation between the discharge and the depth at the outlet. There is no reflected wave in the case of a free outfall.

3. The controlled-outlet conditions at which the depth and discharge may be related through an exponential relation. Although they are not mathematically different from the free-outfall conditions, they produce a different physical effect in the form of a reflected wave moving in the opposite direction of the main flow.

4. Changes in conduit geometry result in local losses. These concentrated energy losses are not accounted for in conduit friction factors and in the unsteady flow equations, thus they may be considered as boundary conditions. These boundary conditions are then used to integrate both flows upstream and downstream of these geometric singularities. A change in boundary geometry may result in one of the two alternatives. One alternative is in flow passing through the critical flow at geometric singularities. In this case the boundary conditions upstream of the boundary singularities are the same as described under (1). The downstream boundary conditions are then the same as those described under point (3). The second alternative is in the flow not passing through the critical stage. In this case the relation between the upstream and downstream depths and the corresponding energy loss at singularities must be known. This relation of energy loss to the two depths produce the boundary conditions in the solution of partial differential equations of unsteady flow.

5. A moving hydraulic jump, a bore, or a breaking wave may also be considered as boundary conditions. The previous four dictates of boundary conditions were considered to be fixed in space. Similar moving boundary conditions exist in the case of moving mechanisms along the conduit with energy dissipation. In this case, it is necessary to determine whether the jump, the bore, or the breaking wave exists at each point of the conduit in time and space. If these conditions exist, then the appropriate energy loss relations are applied as boundary conditions.

The preceding five aspects of boundary conditions have presumed that the condition of sub-critical flow exists in at least one of the regions of unsteady flow. For the condition of super-critical flow throughout the conduit region, including both the inlet and outlet flow conditions, both of the required boundary conditions occur at the same space location. Solving the unsteady flows equations require that these boundary conditions relate depth and discharge as functions of time. An acceptable alternative is an expression for depth as a function of discharge which in turn is a function of time. The mathematical representative of this relation is readily available. However, the physical situations that produce these relations may be of various types. One possible physical reproduction of these conditions is an undershot gate with its rate of rise controlling the depth as a function of time. To obtain the discharge also as a function of time requires a time-varying head on the gate, which is independent of the gate opening rate. Boundary conditions for super-critical flow are not readily reproduced in physical experimentation.

Storm drains for urban or highway drainage may have any of the above five boundary conditions. Also, pumping storm waters into or out of a drainage system may meet any one of the discussed cases of boundary conditions. Apart from energy losses at junction boxes, the boundary conditions discussed in Chapter 4, the only two boundary conditions discussed in this chapter are: (a) the inflow hydrograph, and (b) a depth-time or depth-discharge relation at either the upstream or downstream end of the reach. The selection of the location of this latter condition depends on whether the base flow is in the super-critical or the sub-critical regime. The following discussion relates to the sub-critical flow, in which case the second boundary condition is at the downstream end. The physical condition then may best be expressed as a depth versus discharge relation.

For a free outfall the depth was assumed as the critical depth, so the initial water surface profile was that of a drawdown profile. The location of critical depth as normally computed does not occur at the end of the physical conduit but at some distance upstream. Subchapter 6.2 describes the procedure used to evaluate this distance.

The second boundary condition imposed in the experiments at the downstream end was that of a restricted opening. This insured that the depth of flow was always greater than the normal depth. This produced an initial condition of a backwater surface profile. Subchapter 6.3 describes this boundary condition.

6.2 Free Outfall Boundary Conditions

Definitions and assumptions. The free outfall at the downstream end of a prismatic channel may be considered as that condition for which the total energy of flow is at a minimum for a given discharge. Mathematically this condition may be expressed by

$$\frac{Q^2 B}{gA^3} = 1 \quad , \tag{6.1}$$

in which Q is the discharge, B is the surface width, A is the cross-sectional area, and g is

the gravitational acceleration. This expression is based on two assumptions, namely, the pressure distribution is hydrostatic, and the kinetic energy may be expressed through the mean velocity.

The first assumption is invalidated in the vicinity of the free outfall because of the significant curvature of streamlines. Furthermore, the pressure at the bottom of the end cross section must be atmospheric, or the relative pressure is zero. Thus, the potential portion of the total energy head, relative to the channel bottom, is actually less than that assumed in the development of Eq. 6.1.

The second assumption depends on a uniform velocity distribution in the cross section. The more the velocity distribution differs from the uniform distribution for the same mean velocity, the greater will be the true kinetic energy as compared to the assumed kinetic energy. Based on the previous evaluation of the velocity distribution coefficient α being close to one, it may be assumed that this second assumption is acceptable.

Experimental observations and results. The purpose of taking experimental measurements was to determine the location of critical depth as compared to the depth computed from Eq. 6.1. This position then served as the location of the downstream boundary. Water-surface profiles were measured for a range of discharges from 2.10 to 16.62 cfs. The channel slope ranged from 0.000032 to 0.001022.

Table 6.1 presents the 14 conditions of discharge and slope and the corresponding ratios of end depth to the computed critical depth. Figure 6.1 presents the water-surface profiles for the same conditions along with the locations of the computed critical depths.

TABLE 6.1. Observed end to critical depth ratios. Data values of free outfall (diameter 2.926 ft).

Run No.	Slope	Discharge	y_e/y_c
D1A	.001022	2.10	0.731
S2-9	.000132	3.26	0.746
S1-5	.000032	4.14	0.758
D2A	.001022	4.58	0.749
S1-6	.000032	7.96	0.776
S3-9	.000520	7.98	0.764
D3A	.001022	8.26	0.751
S1-7	.000032	11.98	0.761
D4A	.001022	12.92	0.740
S3-10	.000520	15.97	0.739
D5A	.001022	16.02	0.752
S1-8	.000032	16.04	0.726
S2-10	.000132	16.64	0.753
S1-9	.000032	19.62	0.761
		Mean =	0.750

Conclusions. Within the range of observed end depths, the mean ratio of end-depth to critical depth is 0.750. The ratios tend to be smaller than the mean ratio for the lower depths. The location of computed critical depths from the conduit end varied from less than 3.5 times the critical depth to almost 5.5 times the critical depth. A location of 4.5 times the critical depth was considered typical and was used in the subsequent computations of solution of partial differential equations of unsteady flow. This reduction of the integration length for the numerical solution of unsteady flow is probably insignificant and could be safely ignored in application.

6.3 Controlled Outfall Conditions

Mathematical simulation of the downstream boundary conditions for controlled outflows required the calibration of an end restriction. Any geometric configuration was acceptable providing it satisfied certain criteria:

1. The discharge as a function of depth can be expressed simply by $Q = my^n$, in which m and n are constants and y is the depth of flow upstream of the restriction.

2. The restriction is not great enough to cause the conduit to flow full under the maximum anticipated hydrograph discharge.

3. The velocity distribution of approaching flow is symmetrical and does not differ appreciably from the undisturbed flow.

These criteria were satisfied by restriction consisting of five 7-inch vertical wooden slats held in position by 2.5-inch wide vertical aluminum H-sections. The clear opening was 5 inches between supports. The discharge could thus be controlled by varying the vertical position or by removing one or more of the slats.

Calibration of various combinations of openings was made by measuring the water surface elevation approximately 20 feet upstream of the control and the corresponding discharge. For the range of discharges anticipated in the unsteady flow runs it was concluded that the best combinations of openings was with the three center slats removed.

For this condition the relation between discharge and depth was determined to be

$$Q = 4.84\ y^{1.35} \qquad (6.2)$$

This relation was applied for depths between approximately one-third and eight-tenths of the full diameter. and at 20 feet upstream from the conduit end (the 802.71 ft. station).

This gate configuration and the relation of Eq. 6.2 were used for all subsequent boundary condition evaluations in which the backwater profiles were the initial condition. No attempt was made to modify this steady state relation for the unsteady flow state.

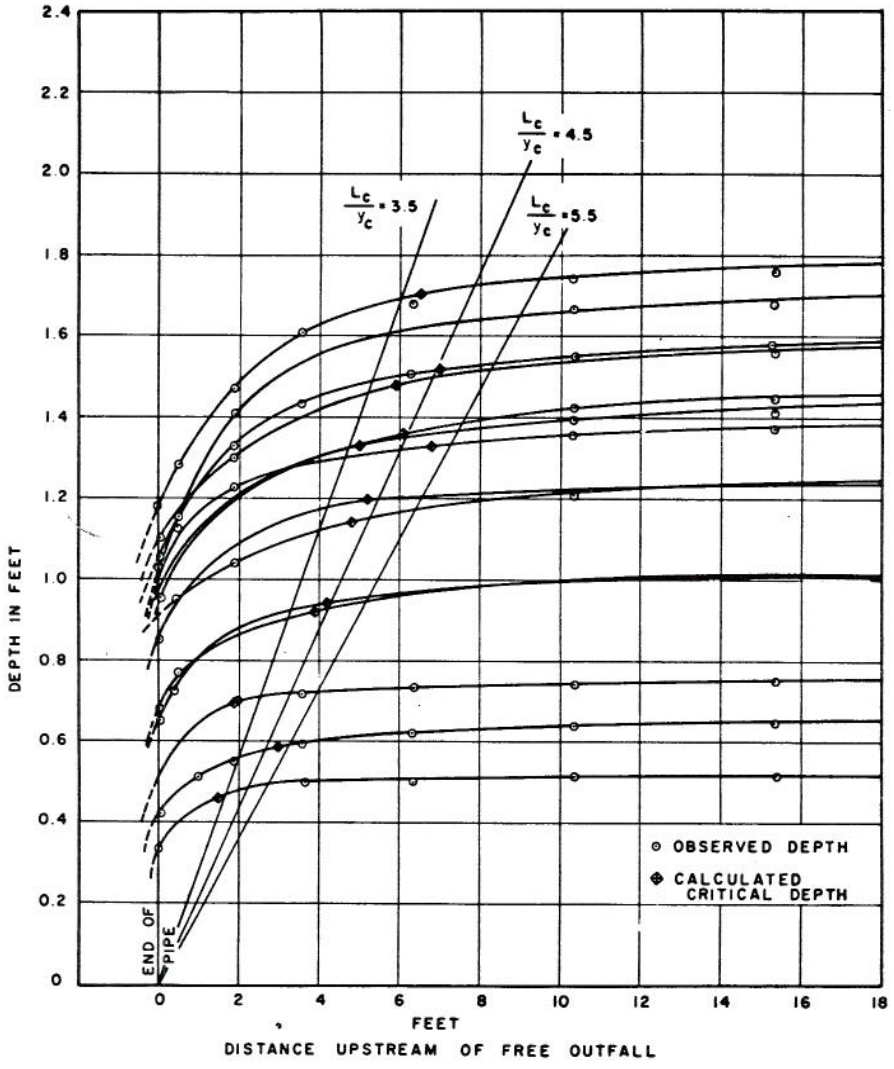

Fig. 6.1. Location of critical depth at the free outfall of a circular cross section.

Chapter 7

INITIAL CONDITIONS FOR EXPERIMENTS AND NUMERICAL INTEGRATIONS

7.1 Definition of Initial Conditions

The integration of the two partial differential equations of gradually varied free-surface steady flow requires that the initial values of velocity and depth be known at a given position in time and space. These values are independent of the insuing solutions and may be arbitrarily established, Realistically, these initial conditions should be the result of physical initial conditions.

For this study the initial conditions are the non-uniform steady flow of the hydrograph base discharge. A mathematical expression for this condition is the ordinary differential equation.

$$\frac{dy}{dx} = \frac{S_o - S_f}{1 + \frac{d}{dy}\left(\frac{\alpha Q^2}{2gA^2}\right)}, \qquad (7.1)$$

in which y is the depth at the position x, x is the distance along the channel, S_o is the bed slope, S_f is the friction slope, α is the energy velocity distribution coefficient, Q is the steady discharge of the hydrograph, A is the cross-sectional area, and g is the gravitational acceleration.

The slope of the energy gradient, S_f, was evaluated by the Darcy-Weisbach equation based on the friction factor evaluation described in Chapter 3.

Comparisons were made between the computed and the observed water-surface profiles for non-uniform steady flow. The objective of these comparisons was to test the validity of the theoretical and numerical determinations of initial conditions.

7.2 Computational Procedure and Results

Determining the depth at specified positions along the conduit was accomplished by a Newton-Raphson iteration of Eq. 7.1 to a tolerance of 0.001 foot of depth. The given information included discharge Q, channel slope S_o, friction factor f, velocity distribution coefficient α, position x along the conduit of points of observed depth, and observed or critical depth at the extreme downstream position. The depth of flow in feet was observed at the following eight positions with respect to the upstream end of the conduit: 20.00, 197.92, 406.07, 509.64, 613.20, 707.71, 772.71, and 821.00.

The boundary conditions for the determination of the steady non-uniform flow as initial conditions were established:

(a) for the mild slope profiles at depths greater than the normal depth (M-1 type curves) the observed depth at the 802.71-foot station was used, and

(b) for the mild slope profiles at depths between the critical and the normal depth (M-2 type curves) the computed critical depth at a position of 4.5 times the critical depth upstream of the conduit end was used.

The root-mean-square (RMS) deviation between the observed and computed depths was computed for three different values of α (1.00, 1.02, and 1.05), and three values of f (.011, .012, and .013). The α-values were selected on:

(a) the usually assumed value of 1.00 in lieu of better information as to its true value;

(b) the value of 1.02 as a representative of the values within the range of expected depths, and

(c) the value of 1.05 as being an extreme for the flow in a uniform conduit with free-surface water flow.

The friction factors were selected according to the most reliable constant value throughout the range of expected depths and velocities, and approximately 10 percent more and less this constant value. It was to be expected that these values would include an engineering estimate of the best constant value for the friction factor of smooth conduits in the expected range of Reynolds numbers. The results of these computations are given in Tables 7.1 and 7.2.

The invert of the experimental conduit deviated from a mathematically uniform slope as indicated in Table 2.3. Since the actual depth of flow above this slightly irregualr invert may not be expected to agree with the computed depth, an adjusted depth was computed at each position. The adjusted depth was based on the depth that would have occurred with the same total energy but with the invert on the mean slope. The root-mean-square deviations for the adjusted depths are given in Tables 7.4 and 7.5.

7.3 Discussion of Comparison of Backwater Calculations

The data presented in Tables 7.1 and 7.2 were analyzed in terms of the mean values of the root-mean-square deviations for each friction factor and α-coefficient. The consolidated results are presented in Tables 7.3 and 7.4. These results do not indicate any strong tendency for a smaller root-mean-square deviation for the friction factor and α- coefficients previously estimated for this conduit, i.e., 0.012, and 1.02. A representative root-mean-square deviation for the conditions observed is approximately 0.025 foot for both the M-1 and M-2 type surface profiles of backwater curves. There is a larger spread of deviations for changes in the friction factor than for changes in the velocity distribution coefficient α.

7.4 Conclusions

Based on the preceding results, it is concluded that a steady non-uniform water-surface profile can be accurately computed as the initial conditions for the solution of unsteady flow equations. It is also concluded that the evaluation of the friction factors is more important than the evaluation of velocity distribution coefficients. The solutions of these equations utilize the variation of the friction factor with the Reynolds number, as given in Chapter 3, to compute S_f of Eq. 7.1. Since the variation of velocity distribution coefficients did not produce significant differences in solutions of unsteady flow equations, subsequent computations utilize an α-value of one in Eq. 7.1.

TABLE 7.1. The root-mean-square deviations for M-1 type backwater curves with the normal depth smaller than the initial depth

Run No.	Q cfs	Normal Depth ft	Initial* Depth ft	α = 1.00			α = 1.02			α = 1.05			f	Slope
				Critical Depth	RMS Dev. Actual	RMS Dev. Adjusted	Critical Depth	RMS Dev. Actual	RMS Dev. Adjusted	Critical Depth	RMS Dev. Actual	RMS Dev. Adjusted		
S3-3	14.10	1.834	2.074	1.205	0.075	0.077	1.211	0.074	0.074	1.220	0.075	0.074	0.011	0.000520
S3-5	7.96	1.269	1.554	0.896	0.034	0.034	0.900	0.034	0.034	0.907	0.034	0.034	0.011	
S3-6	6.21	1.097	1.107	0.788	0.034	0.034	0.792	0.034	0.034	0.798	0.034	0.034	0.011	
S3-7	2.04	0.594	1.028	0.446	0.016	0.014	0.448	0.019	0.016	0.452	0.019	0.016	0.011	
S3-8	1.42	0.490	0.621	0.371	0.025	0.024	0.373	0.025	0.025	0.376	0.025	0.025	0.011	
S3-3	14.10	1.893	2.074	1.205	0.066	0.065	1.211	0.067	0.065	1.220	0.066	0.065	0.012	
S3-5	7.96	1.303	1.554	0.896	0.027	0.026	0.900	0.021	0.026	0.907	0.027	0.025	0.012	
S3-7	2.04	0.608	1.028	0.446	0.017	0.016	0.448	0.017	0.016	0.452	0.018	0.016	0.012	
S3-8	1.42	0.501	0.621	0.371	0.022	0.029	0.373	0.023	0.023	0.376	0.022	0.023	0.012	
S3-3	14.10	1.950	2.074	1.205	0.061	0.058	1.211	0.059	0.058	1.220	0.060	0.058	0.013	
S3-5	7.96	1.335	1.554	0.896	0.022	0.021	0.900	0.022	0.021	0.907	0.022	0.020	0.013	
S3-7	2.04	0.621	1.028	0.446	0.018	0.015	0.448	0.018	0.015	0.452	0.018	0.015	0.013	
S3-8	1.42	0.512	0.621	0.371	0.020	0.020	0.373	0.020	0.020	0.376	0.020	0.020	0.013	
X6A	13.20	1.415	1.441	1.164	0.027	0.040	1.170	0.029	0.040	1.179	0.029	0.040	0.011	0.001001
X6B	13.20	1.415	1.757	1.164	0.016	0.032	1.170	0.017	0.032	1.179	0.016	0.033	0.011	
X6C	13.20	1.415	2.379	1.164	0.021	0.020	1.170	0.021	0.020	1.179	0.021	0.020	0.011	
X9A	20.30	1.884	2.341	1.457	0.062	0.060	1.465	0.067	0.062	1.476	0.067	0.062	0.011	
X10B	16.00	1.599	1.990	1.287	0.042	0.039	1.293	0.041	0.039	-----	-----	-----	0.011	
X12A	8.20	1.066	1.697	0.909	0.022	0.024	0.914	0.023	0.024	-----	-----	-----	0.011	
X12B	8.20	1.066	1.104	0.909	0.014	0.012	0.914	0.014	0.035	-----	-----	-----	0.011	
X6B	13.20	1.454	1.757	1.164	0.023	0.020	1.170	0.022	0.020	1.179	0.022	0.020	0.012	
X6C	13.20	1.454	2.379	1.164	0.021	0.018	1.170	0.021	0.017	0.179	0.020	0.018	0.012	
X9A	20.30	1.945	2.341	1.457	0.023	0.020	1.465	0.077	0.064	1.476	0.071	0.073	0.012	
X10B	16.00	1.646	1.990	1.287	0.050	0.042	1.293	0.048	0.042	1.303	0.047	0.041	0.012	
X12A	8.20	1.093	1.697	0.909	0.019	0.017	0.914	0.019	0.018	0.921	0.019	0.018	0.012	
X12B	8.20	1.093	1.104	0.909	0.018	0.026	0.914	0.018	0.026	0.921	0.015	0.026	0.012	
X12C	8.20	1.093	1.109	0.909	0.015	0.028	0.914	0.015	0.028	-----	-----	-----	0.012	
X13A	4.68	0.798	0.833	0.681	0.018	0.030	-----	-----	-----	-----	-----	-----	0.012	
X13B	4.68	0.798	1.079	0.681	0.013	0.022	-----	-----	-----	-----	-----	-----	0.012	
X12C	8.20	1.093	1.109	-----	-----	-----	0.914	0.015	0.028	-----	-----	-----	0.012	
X12D	8.21	1.093	1.053	-----	-----	-----	0.915	0.044	0.040	-----	-----	-----	0.012	
X6B	13.20	1.491	1.757	1.164	0.033	0.026	1.170	0.035	0.026	1.179	0.032	0.026	0.013	
X6C	13.20	1.491	2.379	1.164	0.026	0.022	1.170	0.026	0.022	0.179	0.026	0.022	0.013	
X9A	20.30	2.006	2.341	1.457	0.044	0.045	1.465	0.046	0.045	1.476	0.091	0.080	0.013	
X10B	16.00	1.690	1.990	1.287	0.060	0.054	1.293	0.060	0.053	1.303	0.059	0.053	0.013	
X12A	8.20	1.119	1.697	0.909	0.0024	0.021	0.914	0.023	0.020	0.921	0.022	0.018	0.013	
D4C	12.92	1.388	2.225	1.151	0.026	0.026	1.157	0.027	0.027	1.166	0.028	0.028	0.011	
D6C	20.51	1.883	2.253	1.465	0.040	0.040	1.473	0.040	0.040	1.484	0.041	0.042	0.011	
D1C	2.10	0.516	1.417	0.453	0.020	0.023	-----	-----	-----	0.458	0.021	0.023	0.012	
D2C	4.58	0.784	2.293	0.674	0.011	0.010	-----	-----	-----	-----	-----	-----	0.012	
D4C	12.92	1.425	2.225	1.151	0.016	0.016	-----	-----	-----	1.166	0.017	0.017	0.012	
D6C	20.51	1.945	2.253	1.465	0.025	0.024	1.473	0.025	0.024	1.484	0.025	0.023	0.012	
D1C	2.10	0.527	1.417	0.453	0.019	0.022	0.455	0.020	0.022	-----	-----	-----	0.013	
D2C	4.58	0.801	2.293	0.674	0.011	0.010	0.677	0.011	0.012	0.682	0.011	0.010	0.013	
D4C	12.92	1.462	2.225	1.151	0.012	0.011	1.157	0.012	0.011	1.166	0.011	0.011	0.013	
D6C	20.51	2.006	2.253	1.465	0.027	0.026	1.473	0.027	0.026	1.484	0.027	0.025	0.013	
D1C	2.10	0.504	1.417	-----	-----	-----	0.455	0.021	0.024	-----	-----	-----	0.011	
D2C	4.58	0.766	2.293	-----	-----	-----	0.677	0.012	0.011	-----	-----	-----	0.011	

*Observed depth at the 802.71 ft. station.

TABLE 7.2. The root-mean-square deviations for M-2 type backwater curves with the normal depth greater than the initial depth

Run No.	Q cfs	Normal Depth ft	Observed values of Initial Depth ft	α = 1.00			α = 1.02			α = 1.05			f	Slope
				Critical Depth	RMS Dev. Actual	RMS Dev. Adjusted	Critical Depth	RMS Dev. Actual	RMS Dev. Adjusted	Critical Depth	RMS Dev. Actual	RMS Dev. Adjusted		
S3-4	14.41	1.863	1.768	1.218	0.040	0.036	1.225	0.040	0.036	1.234	0.040	0.036	0.011	0.000520
S3-4	14.41	1.923	1.768	1.218	0.042	0.038	1.225	0.039	0.039	1.234	0.033	0.041	0.012	
S3-6	6.21	1.125	1.107	0.788	0.026	0.025	0.792	0.025	0.024	0.798	0.026	0.025	0.012	
S3-4	14.41	1.962	1.768	1.218	0.045	0.042	1.225	0.043	0.042	1.234	0.045	0.041	0.013	
S3-6	6.21	1.152	1.107	0.788	0.021	0.019	0.792	0.021	0.024	0.798	0.020	0.019	0.013	
X6-E	13.20	1.415	1.331	1.164	0.028	0.044	1.170	0.028	0.044	1.179	0.027	0.044	0.011	0.001001
X7-A	25.90	2.301	2.122	1.656	0.056	0.051	1.664	0.065	0.059	1.677	0.065	0.052	0.011	
X7-B	25.90	2.301	1.828	1.656	0.055	0.062	1.664	0.066	0.072	1.677	0.067	0.072	0.011	
X7-C	25.90	2.301	1.831	1.656	0.072	0.074	1.664	0.065	0.070	1.677	0.067	0.074	0.011	
X8-B	23.70	2.124	1.753	1.580	0.019	0.042	1.589	0.023	0.043	1.601	0.022	0.043	0.011	
X8-C	23.70	2.124	2.023	1.580	0.027	0.036	1.589	0.027	0.034	1.601	0.026	0.034	0.011	
X9-B	20.30	1.884	1.619	1.457	0.061	0.066	1.465	0.061	0.066	1.476	0.060	0.066	0.011	
X9-C	20.30	1.884	1.832	1.457	0.061	0.061	1.465	0.061	0.061	1.476	0.065	0.060	0.011	
X10-A	16.00	1.599	1.579	1.287	0.013	0.032	1.293	0.013	0.030	1.303	0.013	0.030	0.011	
X10-C	16.00	1.599	1.448	1.287	0.023	0.043	1.293	0.023	0.043	-----	-----	-----	0.011	
X6-A	13.20	1.454	1.441	1.164	0.018	0.024	1.170	0.018	0.025	1.179	0.018	0.025	0.012	
X6-E	13.20	1.454	1.331	1.164	0.020	0.034	1.170	0.020	0.011	1.179	0.020	0.034	0.012	
X8-B	23.70	2.289	1.753	1.580	0.066	0.080	1.589	0.079	0.082	1.601	0.082	0.085	0.013	
X8-C	23.70	2.289	2.023	1.580	0.052	0.047	1.589	0.051	0.048	1.601	0.052	0.048	0.013	
X9-B	20.30	2.006	1.619	1.457	0.098	0.086	1.465	0.091	0.087	1.476	0.095	0.090	0.013	
X9-C	20.30	2.006	1.832	1.457	0.091	0.080	1.465	0.092	0.081	1.476	0.091	0.080	0.013	
X10-A	16.00	1.690	1.579	1.287	0.045	0.043	1.293	0.046	0.042	1.303	0.046	0.043	0.013	
X10-C	16.00	1.690	1.448	1.287	0.048	0.053	1.293	0.049	0.054	1.303	0.050	0.055	0.013	
X12-B	8.20	1.119	1.104	0.909	0.026	0.026	0.914	0.026	0.026	1.303	0.050	0.053	0.013	
D1B	2.10	0.504	0.464	0.453	0.026	0.037	0.455	0.026	0.036	-----	-----	-----	0.011	0.001022
D2A	4.58	0.766	0.696	-----	-----	-----	0.677	0.050	0.056	0.682	0.050	0.055	0.011	
D2B	4.58	0.766	0.724	-----	-----	-----	0.677	0.037	0.040	0.682	0.037	0.037	0.011	
D4B	12.92	1.388	1.292	1.151	0.032	0.037	1.157	0.034	0.035	1.166	0.034	0.034	0.011	
D5B	16.02	1.590	1.490	1.288	0.032	0.033	1.294	0.032	0.032	1.304	0.032	0.032	0.011	
D6B	20.51	1.883	1.737	1.465	0.038	0.038	1.473	0.039	0.040	1.484	0.038	0.038	0.011	
D7B	23.51	2.092	1.926	1.574	0.024	0.024	1.582	0.024	0.024	1.594	0.024	0.024	0.011	
D8B	25.60	2.253	2.029	1.646	0.029	0.029	1.654	0.028	0.028	1.667	0.028	0.028	0.011	
D1B	2.10	0.516	0.464	0.453	0.023	0.034	-----	-----	-----	0.458	0.020	0.036	0.012	
D2A	4.58	0.784	0.696	0.674	0.039	0.044	-----	-----	-----	0.682	0.038	0.044	0.012	
D2B	4.58	0.784	0.724	0.674	0.029	0.033	-----	-----	-----	0.682	0.032	0.033	0.012	
D4B	12.92	1.425	1.292	1.151	0.021	0.020	-----	-----	-----	1.166	0.021	0.020	0.012	
D5B	16.02	1.636	1.490	1.288	0.018	0.017	1.294	0.019	0.017	1.304	0.019	0.016	0.012	
D6B	20.51	1.945	1.737	1.465	0.025	0.023	1.473	0.025	0.023	1.484	0.024	0.023	0.012	
D7B	23.51	2.170	1.926	-----	-----	-----	1.582	0.025	0.022	1.594	0.025	0.023	0.012	
D8B	25.60	2.352	2.029	-----	-----	-----	1.654	0.024	0.018	1.667	0.021	0.018	0.012	
D1B	2.10	0.527	0.464	0.453	0.020	0.034	0.455	0.017	0.032	-----	-----	-----	0.013	
D2A	4.58	0.801	0.696	0.674	0.028	0.034	0.677	0.028	0.035	0.682	0.027	0.035	0.013	
D2B	4.58	0.801	0.724	0.674	0.029	0.025	0.677	0.031	0.025	0.682	0.026	0.023	0.013	
D4B	12.92	1.462	1.292	1.151	0.025	0.024	1.157	0.027	0.025	1.166	0.024	0.020	0.013	
D5B	16.02	1.680	1.490	1.288	0.030	0.026	1.294	0.030	0.027	1.304	0.032	0.028	0.013	
D6B	20.51	2.006	1.737	1.465	0.037	0.035	1.473	0.038	0.035	1.484	0.037	0.035	0.013	
D7B	23.51	2.250	1.926	1.574	0.049	0.048	-----	-----	-----	1.594	0.052	0.050	0.013	
S21	5.61	1.563	1.210	0.748	0.035	0.034	0.752	0.036	0.033	0.757	0.036	0.034	0.011	0.000132
S2-6	4.71	1.400	1.012	0.684	0.035	0.034	0.687	0.034	0.033	0.692	0.034	0.033	0.011	
S2-7	3.44	1.159	0.611	0.582	0.035	0.035	0.585	0.033	0.034	0.590	0.032	0.033	0.011	
S2-8	1.06	0.604	0.339	0.320	0.044	0.042	0.322	0.043	0.041	0.324	0.043	0.040	0.011	
S2-1	5.61	1.608	1.210	0.748	0.029	0.028	0.752	0.030	0.027	0.757	0.030	0.027	0.012	
S2-6	4.71	1.438	1.012	0.684	0.028	0.026	0.687	0.028	0.026	0.692	0.028	0.026	0.012	
S2-7	3.44	1.189	0.611	0.582	0.027	0.027	0.585	0.025	0.025	0.590	0.024	0.025	0.012	
S2-8	1.06	0.618	0.339	0.320	0.037	0.035	0.322	0.038	0.035	0.324	0.037	0.035	0.012	
S2-1	5.61	1.651	1.210	0.748	0.026	0.023	0.752	0.025	0.022	0.757	0.025	0.022	0.013	
S2-6	4.71	1.475	1.012	0.684	0.022	0.020	0.687	0.022	0.020	0.692	0.022	0.020	0.013	
S2-7	3.44	1.218	0.611	0.582	0.020	0.020	0.585	0.018	0.019	0.590	0.017	0.018	0.013	
S2-8	1.06	0.631	0.339	0.320	0.033	0.030	0.322	0.032	0.030	0.324	0.032	0.029	0.013	

TABLE 7.3. Difference in computed and observed depths, root-mean-square values in feet for M-1 type curves

Velocity distribution coefficient	Friction factor f					
	0.011	0.012	0.013	0.011	0.012	0.013
α	Root-mean-square values					
	Unadjusted depth			Adjusted depth		
1.00	0.026	0.020	0.023	0.033	0.023	0.022
1.02	0.024	0.024	0.023	0.033	0.026	0.022
1.05	0.024	0.022	0.024	0.031	0.023	0.021

TABLE 7.4. Difference in computed and observed depths, root-mean-square values in feet for M-2 type curves

Velocity distribution coefficient	Friction factor f					
	0.011	0.012	0.013	0.011	0.012	0.013
α	Root-mean-square values					
	Unadjusted depth			Adjusted depth		
1.00	0.035	0.026	0.030	0.037	0.030	0.034
1.02	0.034	0.025	0.030	0.040	0.026	0.031
1.05	0.036	0.026	0.036	0.041	0.026	0.037

Chapter 8

CONCLUSIONS AND RECOMMENDATIONS

8.1 Conclusions

After considering the analysis and discussion of the various evaluations of geometric and hydraulic parameters in Chapters 2 through 7, the following major conclusions are drawn:

1. Geometric parameters can be well evaluated for the circular storm drain; errors in depth measurements, errors from the assumed ellipticity and inclination of cross sections, and errors from undulation of inverts are all well within tolerable limits.

2. Because the 822-foot experimental storm conduit is a hydraulically smooth pipe, the relation between the Darcy-Weisbach friction factor (f) and the Reynolds number (R_e) may be well approximated by a power function, $f = 0.10939\ R_e^{-0.17944}$, with the Reynolds number in the range 3×10^4 to 6×10^5 for the steady flow conditions. An average Darcy-Weisbach friction factor of 0.012 is a representative value of the conduit roughness, for this range of R_e.

3. Under steady-flow conditions, for the lateral inlet with its upper position in the junction box, the power loss relation for junction box losses is

$$P_r = \frac{-0.482}{Q_r + 0.55} + 0.77 \quad ,$$

and for the lateral inlet with its lower position in the junction box the power loss relation is

$$P_r = \frac{-2.78 + 1.71\ D_r}{Q_r + 3.122 - 0.167\ D_r} + 0.77 \quad .$$

4. The relation between the velocity distribution coefficients, α and β is approximately $(\alpha-1)/(\beta-1) = 3.0$ for the experimental results obtained under the steady-flow conditions, with representative (average) values of $\alpha = 1.03$ and $\beta = 1.01$ for the experimental conditions.

5. The relation between discharge (Q) and depth (y) at the controlled outfall of the conduit for steady flow conditions can be well approximated by an exponential function of the form $Q = my^n$. The values of the constants m and n depend on the shape and size of the arbitrary opening of the controlled outfall.

6. For conduit slope less than 0.001 the mean ratio of end depth to critical depth obtained for the conduit free-water outfall and for the steady-flow conditions is 0.750.

7. By examining the sources of experimental errors, it is possible to establish boundary and initial conditions, with the errors within tolerable limits.

8.2 Recommendations for Further Experimental Research

1. For storm drains of circular cross section the flow characteristics change significantly when the flow is at nearly full pipe because of changes in air pressure. A criterion should be developed to define the applicability of partially full flow in circular conduits when the water surface approaches full conduit.

2. The influence of changes in boundary layers in the unsteady flow regime on the estimation of friction factors and the velocity distribution coefficients suggests that further studies of such effects would be beneficial, with new ideas, different experimentation and new and appropriate instrumentation.

3. The evaluation of flow resistance in this study is limited to turbulent hydraulically smooth boundaries. Similar evaluation should be carried out for turbulent hydraulically rough boundaries.

4. Because storm drains may have sudden changes in physical boundary geometry (such as water drops with partial backwater effects of downstream depths on upstream flow, use of pumps for removing the storm water at particular points, and similar), further investigations should be conducted to properly evaluate these particular boundary conditions.

REFERENCES

1. Henderson, F. M., 1964, Steady Flow in Sinusoidally Varying Channels, Hydraulics and Fluid Mechanics, R. Silvester (Editor), MacMillan Company, New York, pp. 51-67.

2. Committee on Hydromechanics of the Hydraulics Division, 1963, Friction Factors in Open Channels, American Society of Civil Engineers, Journal of Hydraulics Division, Vol. 89, HY2, pp. 97-143.

3. Camp, Thomas R., 1946, Design of Sewers to Facilitate Flow, Sewage Works Journal, Vol. 18, No. 1, pp. 3-16.

4. Rouse, Hunter, 1946, Elementary Mechanics of Fluids, John Wiley & Sons, Inc., New York.

5. Stevens, J. C., 1926, Theoretical Energy Losses in Intersecting Pipes, Engineering News-Record, pp. 140.

6. Taylor, Edward H., 1944, Flow Characteristics at Rectangular Open-Channel Junctions, Transactions, American Society of Civil Engineers, Vol. 109, pp. 893-903.

7. Bowers, Charles E., 1950, Studies of Open-Channel Junctions, Part V of Hydraulic Model Studies for Whiting Field Naval Air Station, Milton, Florida. University of Minnesota, St. Anthony Falls Hydraulic Laboratory, Technical Paper Number 6, Series B.

8. Chow, Ven Te, 1964, Handbook of Applied Hydrology, New York, McGraw-Hill Book Company.

9. Sangster, W. M., Wood, H. W., Smerdon, E. T., and Bossy, H. G., 1958, Pressure Changes at Storm Drain Junctions. The University of Missouri Bulletin, Vol. 59, No. 35, Engineering Experiment Station Series No. 41, Columbia, Mo.

10. Chow, Ven Te, 1959, Open Channel Hydraulics, New York, McGraw-Hill Book Company, 680 pp.

Key Words: Storm Drain, Flood Routing, Geometry, Flow Resistance, Velocity Distribution Coefficients, Junction Box Losses, Steady Non-Uniform Flow.

Abstract: The primary objective of this third part of a four-part series of hydrology papers on flood routing through storm drains is to present results on the investigation of the geometric and hydraulic parameters of the experimental conduit. The errors in cross section geometric parameters are analyzed in a conduit not ideally circular but approximated by an elliptical shape; errors are also analyzed when the undulations in the longitudinal slope of the conduit affect the predicted water surface profiles and thus the geometric parameters for a given water depth. The variation of hydraulic parameter of resistance, expressed by the Darcy-Weisbach friction factor, is experimentally determined and compared to the theoretical relation to Reynolds number. Energy losses in a 90° junction box are studied. The velocity distribution coefficients are shown to vary with the Darcy-Weisbach friction factor, and consequently, with the depth of flow. Boundary conditions for both controlled and free outfall are experimentally determined and approximated by power functions. Two types of steady non-uniform flow profiles, M1 and M2 are observed and analyzed as the initial conditions for the unsteady flow computations.

Reference: Yevjevich, Vujica and Albert H. Barnes, Colorado State University, Hydrology Paper No. 45 (November 1970) "Flood Routing Through Storm Drains, Part III, Evaluation of Geometric and Hydraulic Parameters."

Key Words: Storm Drain, Flood Routing, Geometry, Flow Resistance, Velocity Distribution Coefficients, Junction Box Losses, Steady Non-Uniform Flow.

Abstract: The primary objective of this third part of a four-part series of hydrology papers on flood routing through storm drains is to present results on the investigation of the geometric and hydraulic parameters of the experimental conduit. The errors in cross section geometric parameters are analyzed in a conduit not ideally circular but approximated by an elliptical shape; errors are also analyzed when the undulations in the longitudinal slope of the conduit affect the predicted water surface profiles and thus the geometric parameters for a given water depth. The variation of hydraulic parameter of resistance, expressed by the Darcy-Weisbach friction factor, is experimentally determined and compared to the theoretical relation to Reynolds number. Energy losses in a 90° junction box are studied. The velocity distribution coefficients are shown to vary with the Darcy-Weisbach friction factor, and consequently, with the depth of flow. Boundary conditions for both controlled and free outfall are experimentally determined and approximated by power functions. Two types of steady non-uniform flow profiles, M1 and M2 are observed and analyzed as the initial conditions for the unsteady flow computations.

Reference: Yevjevich, Vujica and Albert H. Barnes, Colorado State University, Hydrology Paper No. 45 (November 1970) "Flood Routing Through Storm Drains, Part III, Evaluation of Geometric and Hydraulic Parameters."

Key Words: Storm Drain, Flood Routing, Geometry, Flow Resistance, Velocity Distribution Coefficients, Junction Box Losses, Steady Non-Uniform Flow.

Abstract: The primary objective of this third part of a four-part series of hydrology papers on flood routing through storm drains is to present results on the investigation of the geometric and hydraulic parameters of the experimental conduit. The errors in cross section geometric parameters are analyzed in a conduit not ideally circular but approximated by an elliptical shape; errors are also analyzed when the undulations in the longitudinal slope of the conduit affect the predicted water surface profiles and thus the geometric parameters for a given water depth. The variation of hydraulic parameter of resistance, expressed by the Darcy-Weisbach friction factor, is experimentally determined and compared to the theoretical relation to Reynolds number. Energy losses in a 90° junction box are studied. The velocity distribution coefficients are shown to vary with the Darcy-Weisbach friction factor, and consequently, with the depth of flow. Boundary conditions for both controlled and free outfall are experimentally determined and approximated by power functions. Two types of steady non-uniform flow profiles, M1 and M2 are observed and analyzed as the initial conditions for the unsteady flow computations.

Reference: Yevjevich, Vujica and Albert H. Barnes, Colorado State University, Hydrology Paper No. 45 (November 1970) "Flood Routing Through Storm Drains, Part III, Evaluation of Geometric and Hydraulic Parameters."

Key Words: Storm Drain, Flood Routing, Geometry, Flow Resistance, Velocity Distribution Coefficients, Junction Box Losses, Steady Non-Uniform Flow.

Abstract: The primary objective of this third part of a four-part series of hydrology papers on flood routing through storm drains is to present results on the investigation of the geometric and hydraulic parameters of the experimental conduit. The errors in cross section geometric parameters are analyzed in a conduit not ideally circular but approximated by an elliptical shape; errors are also analyzed when the undulations in the longitudinal slope of the conduit affect the predicted water surface profiles and thus the geometric parameters for a given water depth. The variation of hydraulic parameter of resistance, expressed by the Darcy-Weisbach friction factor, is experimentally determined and compared to the theoretical relation to Reynolds number. Energy losses in a 90° junction box are studied. The velocity distribution coefficients are shown to vary with the Darcy-Weisbach friction factor, and consequently, with the depth of flow. Boundary conditions for both controlled and free outfall are experimentally determined and approximated by power functions. Two types of steady non-uniform flow profiles, M1 and M2 are observed and analyzed as the initial conditions for the unsteady flow computations.

Reference: Yevjevich, Vujica and Albert H. Barnes, Colorado State University, Hydrology Paper No. 45 (November 1970) "Flood Routing Through Storm Drains, Part III, Evaluation of Geometric and Hydraulic Parameters."

PREVIOUSLY PUBLISHED PAPERS

Colorado State University Hydrology Papers

No. 27 "Diffusion of Entrapped Gas From Porous Media," by Kenneth M. Adam and Arthur T. Corey, April 1968.

No. 28 "Sampling Bacteria in a Mountain Stream," by Samuel H. Kunkle and James R. Meimann, March 1968.

No. 29 "Estimating Design Floods From Extreme Rainfall," by Frederick C. Bell, July 1968.

No. 30 "Conservation of Ground Water by Gravel Mulches," by A.T. Corey and W.D. Kemper, May 1968.

No. 31 "Effects of Truncation on Dependence in Hydrologic Time Series," by Rezaul Karim Bhuiya and Vujica Yevjevich, November 1968.

No. 32 "Properties of Non-Homogeneous Hydrologic Series," by V. Yevjevich and R.I. Jeng, April 1969.

No. 33 "Runs of Precipitation Series," by Jose Llamas and M.M. Siddiqui, May 1969.

No. 34 "Statistical Discrimination of Change in Daily Runoff," by Andre J. Dumas and Hubert J. Morel-Seytoux, August 1969.

No. 35 "Stochastic Process of Precipitation," by P. Todorovic and V. Yevjevich, September 1969.

No. 36 "Suitability of the Upper Colorado River Basin for Precipitation Management," by Hiroshi Nakamichi and Hubert J. Morel-Seytoux, October 1969.

No. 37 "Regional Discrimination of Change in Runoff," by Viboon Nimmannit and Hubert J. Morel-Seytoux, November 1969.

No. 38 "Evaluation of the Effect of Impoundment on Water Quality in Cheney Reservoir," by J.C. Ward and S. Karaki, March 1970.

No. 39 "The Kinematic Cascade as a Hydrologic Model," by David F. Kibler and David A. Woolhiser, February 1970.

No. 40 "Application of Run-Lengths to Hydrologic Series," by Jaime Saldarriaga and Vujica Yevjevich, April 1970.

No. 41 "Numerical Simulation of Dispersion in Groundwater Aquifers," by Donald Lee Reddell and Daniel K. Sunada, June 1970.

No. 42 "Theoretical Probability Distributions for Flood Peaks," by Emir Zelenhasic, November 1970.

No. 43 "Flood Routing Through Storm Drains, Part I, Solution of Problems of Unsteady Free Surface Flow in a Storm Drain", by V. Yevjevich and A.H. Barnes, November 1970.

No. 44 "Flood Routing Through Storm Drains, Part II, Physical Facilities and Experiments", by V. Yevjevich and A.H. Barnes, November 1970.